Dynamics of mRNA fate during light stress and recovery: from transcription to stability and translation

Aaron B. Smith[1#], Diep R. Ganguly[1,2#], Marten Moore[1], Andrew F. Bowerman[1], Barry J. Pogson[1,3]*, Peter A Crisp[4]*
[1] Research School of Biology, The Australian National University, Acton, Canberra, ACT, 2601, Australia.
[2] CSIRO Synthetic Biology Future Science Platform
[3] Australian Research Council Training Centre For Future Crops
[4] School of Agriculture and Food Sciences, The University of Queensland, Brisbane QLD 4072, Australia

ORCIDs: 0000-0002-5828-0039 (ABS), 0000-0001-6746-0181 (DRG), 0000-0002-3423-2403 (MM), 0000-0003-1729-7843 (AFB), 0000-0003-1869-2423 (BJP), 0000-0002-3655-0130 (PAC)
#These authors contributed equally
***Correspondence**: peter.crisp@anu.edu.au, barry.pogson@anu.edu.au
Key words: mRNA stability, light stress, recovery, *Arabidopsis thaliana*
Author contributions: ABS, BJP, and PAC conceived the project and designed experiments. ABS and DRG performed *in planta* cordycepin experiments and mRNA sequencing. ABS and MM performed polysome profiling. ABS, DRG, and AFB performed data analysis. ABS and DRG led manuscript preparation. All authors read and commented on the manuscript.

Abstract

The stability of mRNA is an important determinant of its abundance and, consequently, protein production. There has been extensive research on the pathways governing mRNA stability and translation, however, it is unclear the extent to which these processes are modulated by environmental conditions. We previously modelled rapid recovery gene down-regulation (RRGD) following light stress in *Arabidopsis thaliana* (Arabidopsis) using mathematical calculations to account for transcription in order to predict half-lives and led to the hypothesis of recovery-specific transcript destabilisation. Here, we test this hypothesis by quantifying changes in transcription, mRNA stability, and translation in leaves of mature Arabidopsis undergoing light stress and recovery and investigate processes regulating transcript abundance and fate. Compared to juvenile plants from prior work, here we find that stability is altered for a range of transcripts that encode proteins involved in post-transcriptional processes in mature leaves. We also observe transcript destabilisation during light stress, followed by re-stabilisation upon recovery. Alongside this, we observe fast transcriptional shut-off in recovery that, when paired with transcript destabilisation, promotes rapid down-regulation of stress-induced genes. Translation was dynamic over the course of light stress and recovery, with substantial transcript-specific increases in polysome loading observed during late stress independently of total mRNA abundance. Taken together, we provide evidence for the combinatorial regulation of transcription, mRNA stability, and translation that occurs during light stress and recovery.

Introduction

Responses to stress have been the subject of much research; however, the post-stress recovery phase has been understudied and is likely to be equally complex and dynamic. Often, the molecular changes that occur at the onset of stress are protective in nature and divert resources away from growth and reproduction. Recovery, therefore, serves the purpose of resetting these processes in order to maximise growth potential. A balance is, therefore, required between such resetting and a competing process of consolidation ('memory') of defences (Crisp et al. 2016; Bäurle and Trindade 2020). Nonetheless, it may be counter-productive to maintain protective mechanisms indefinitely, as demonstrated by the growth penalty incurred by some stress tolerant plant lines (Mickelbart et al. 2015). For instance, activity of the K^+/H^+ antiporter KEA3 was found to be important for relaxation of the energy-dependent portion of non-photochemical quenching (qE) following light stress (Armbruster et al. 2014). Increasing *KEA3* expression resulted in faster qE relaxation resulting in enhanced photosystem II efficiency (Armbruster et al. 2016). This example highlights the potential in optimising stress recovery for crop improvements.

Transcriptome resetting has been characterised during recovery from multiple stressors. For example, sulphur starvation in Arabidopsis led to the up-regulation of many sulphur metabolism-associated genes, which returned to pre-stress levels within three hours of resupply (Bielecka et al. 2014). Recovery of rice to phosphate starvation occurred within one day of resupply, although full recovery took 31 days in line with re-establishing original phosphate content (Secco et al. 2015). On the other hand, rice recovered from submergence within hours (Locke et al. 2018). We previously reported on rapid transcriptome resetting in Arabidopsis following light stress, whereby stress-induced mRNAs were down-regulated to pre-stress levels within 30 minutes; a phenomenon termed RRGD (Crisp et al. 2017). Of note was the observation that RRGD loci exhibited far shorter half-lives during recovery compared to steady state measurements (Narsai et al. 2007), suggesting specific destabilisation. The ability to rapidly alter the composition of the transcriptome gains particular importance during stress, when factors such as dehydration, heat, and oxidative stress can cause extensive cellular damage. While transcription can be adjusted to produce stress-associated transcripts, post-transcriptional changes, including modulating mRNA stability, are likely to permit faster changes in abundance; a valuable feature when a rapid response is required (Pérez-Ortín et al. 2007). Subtle shifts in stability can also greatly affect the ultimate number of mRNA molecules per cell over time (Ross 1995). It is worth noting that recovery is more than just resumption of pre-stress gene regulation, as a diversity of recovery-induced gene expression programs are evident (Yeung et al. 2018; Crisp et al. 2017). For example, the down-regulation of stress-induced transcripts during recovery is accompanied by the up-regulation of distinct genes, the products of which may play roles in recovery. This includes genes encoding RNA decay factors, such as the deadenylase-encoding *CAF1* (Crisp et al. 2017). Whether these transcripts are translated proportional to their up-regulation is unclear, but it may indicate a rapid means of re-establishing pre-stress cellular conditions.

There are increasing observations of changes in mRNA stability during plant stress responses. Under high salinity, N^6-methyladenosine promotes stabilisation of transcripts encoding salinity-associated proteins (Kramer et al. 2020). Conversely, salinity also induces siRNA-mediated degradation of *P5CDH* transcripts to promote proline accumulation that aids in salinity tolerance, representing an instance of preferential destabilisation (Borsani et al. 2005). During cold stress, the interplay between changes in DNA transcription and mRNA stability and transcription culminate into faster changes in overall expression of cold-responsive genes (Arae et al. 2017). Transcript degradation during stress appears to utilise the 5′ → 3′ decay pathway through the activity of decapping factors (DCP1, DPC2, DCP5, and VCS) and XRN4, including in thermal acclimation (Merret et al. 2013; Nguyen et al. 2015), photomorphogenesis (Jang et al. 2019), pathogen resistance (Yu et al. 2019), ABA signalling (Wawer et al. 2018), and dehydration or osmotic stress (Xu and Chua 2012; Soma et al. 2017). Nuclear XRNs have also been associated with elevated drought tolerance, due to inhibition by SAL1-PAP signalling promoting RNA polymerase II read-through into stress-associated genes (Estavillo et al. 2011; Crisp et al. 2018). These studies highlight the biological importance and potential specificity of the RNA decay machinery.

Translation is intimately tied with RNA decay in both cooperative and antagonistic ways (Roy and Jacobson 2013). Competition for the 5′ cap can be a key determinant of mRNA stability, and high ribosome density and translation speed can be an indicator of elevated stability (Chan et al. 2018; Hanson et al. 2018; Schwartz and Parker 2000). Conversely, co-translational decay mechanisms are utilised to degrade transcripts on which ribosomes are stalled or elongating at a slowed rate, thereby permitting ribosome recycling (Merret et al. 2015; Pelechano et al. 2015). Previously, evidence of co-translational decay in Arabidopsis plants undergoing light stress and recovery suggested that light-induced transcripts could be degraded while still polysome-bound, bypassing the need for dissociation from ribosomes (Crisp et al. 2017). During heat stress, for example, a dramatic increase in monosomal loading relative to polysome loading is observed, which dissipates during recovery (Merret et al. 2017).

Preferential translation may permit a cell to make rapid changes in protein levels independently of transcription (Muñoz and Castellano 2012). As prioritisation of energy and resources is often paramount during adverse conditions, translation is often repressed globally with the exception of a subset of transcripts required for stress responses (Chen et al. 2021; Juntawong et al. 2014). The repression of translation can involve degradation or transcriptional repression of genes encoding ribosomal proteins or translational factors (Sheikh et al. 1999; Munchel et al. 2011); however, a more rapid response is facilitated through dissociation of transcripts from initiation factors and ribosomes (Liu and Qian 2014; Bresson et al.

2020). In many cases, the disassembly of polysomes is associated with formation of cytoplasmic foci called stress granules, which store complexes of translationally-inert mRNAs, translation initiation factors, and other RNA-binding proteins thereby preventing their shuttling to, and degradation at, processing bodies (Chantarachot and Bailey-Serres 2018). Upon removal of the stress, transcriptional up-regulation of the translation machinery occurs presumably in order to resume pre-stress protein production (Yeung et al. 2018). This may be aided by the release of transcripts encoding ribosomal proteins from stress granules. For example Arabidopsis heat shock proteins regulate the disassembly of stress granules following heat stress, allowing stored mRNAs encoding initiation factor complexes to commence translation (Merret et al. 2017).

We hypothesise that mRNA stability and translation are combinatorially modulated during recovery from light stress, which contributes to the resetting of protective mechanisms by shaping the cellular RNA pool available for translation. Previously, we did not assess whether the stability of individual transcripts shifted between unstressed, stressed, and recovery. An ongoing challenge with examining mRNA stability during stress is delineating changes in stability from changes in transcription. Accurate measurements of RNA decay requires either cessation of transcription through the use of transcriptional inhibitors, or *in vivo* labelling of mRNAs. The treatment of plants undergoing stress is limited by the nature and duration of the stress being examined. For example, delivery of RNA analogs via root feeding requires at least one hour (Szabo et al. 2020); unsuitable for short term, transient stresses such as high light in which the transcriptome changes within minutes. Previous attempts to model RNA half-life in the absence of these treatments has had some success, but was heavily limited to up-regulated transcripts that displayed stepwise reductions in abundance (Crisp et al. 2017).

To address the aforementioned shortcomings in prior reports, we established a method to perform transcriptional inhibition in leaves of mature soil-grown plants using syringe-infiltration of the transcriptional inhibitor, cordycepin. This enabled us to compare genome-wide changes in mRNA stability between stress and recovery conditions *in situ*. We paired these with measurements of precursor mRNA (pre-mRNA) levels, as a proxy for transcriptional changes; and with translation rates, by profiling ribosome-bound mRNA during light stress and recovery. This combinatorial strategy revealed that RRGD was facilitated by interplay between regulation of transcription and mRNA stability. Whilst total mRNA abundance tracked with polysome-bound RNA levels (i.e. translation), this relationship was uncoupled during late light stress and early recovery, suggesting the occurrence of translational re-organisation.

Materials and Methods

Plant growth and treatments

Arabidopsis seeds were sown onto moist soil (Martins Seed Raising and Cutting Mix) supplemented with Osmocote Exact Mini slow release fertiliser (Scotts) at 1 g/L dry volume of soil and 1 L of 0.3 % (v/v) AzaMax (Organic Crop Protectants). Seeds were covered with plastic wrap and stratified at 4 °C in the dark for at least 72 hours to break dormancy and synchronise germination. Stratified seeds were transferred to a temperature controlled Conviron S10H growth chamber (Conviron, Canada) fitted with a mixture of 250 W metal halide (Venture Lighting, MH 250W/U) and high pressure sodium lamps (Phillips, SON- T 250W E E40 SL/12). Plants were cultivated under a 12-hour photoperiod of 100 µmol photons m^{-2} s^{-1}, 21 °C, and 55 % relative humidity. Plants were watered to saturation the day preceding light stress application. Light stress was induced by increasing the light intensity to 10× growth irradiance (i.e. 1000 µmol photons m^{-2} s^{-1}), resulting in a “hot high light” treatment that effectively induces oxidative stress (Jung et al. 2013). For recovery, plants were returned to pre-stress light conditions. For transcriptional inhibition, cordycepin (3'-deoxyadenosine, Sigma-Aldrich), was syringe-infiltrated on the abaxial side of fully expanded leaves (true leaves 4-6) of 28-day old plants. Individual leaves were infiltrated with 0.1 mL of incubation buffer [1 mM PIPES (pH 6.25), 1 mM sodium citrate, 1 mM KCl, 15 mM sucrose (Seeley et al. 1992)] with 0.6 mM cordycepin, or without (mock), using a 1 mL needleless syringe (Terumo). Excess liquid was removed from the leaf surface and plants were incubated for a minimum of 10 minutes before further treatment and harvesting. Each biological replicate was derived from leaves syringe-infiltrated, with either mock or cordycepin treatment, from the same plant at each time point per condition: unstressed (US), high light

(HL), or recovery (REC). Infiltrated leaves were excised, at the appropriate time point under each condition, from the base of the petiole and immediately flash-frozen, in a 2 mL safe-lock microcentrifuge tube (Eppendorf), using liquid nitrogen. Frozen tissue was stored at -80 °C until ready for processing.

RNA isolation

Frozen tissue was ground into a fine powder using a ⅛" steel ball bearing with 1 min shaking at 25 Hz in a TissueLyser II (Qiagen). Total RNA was extracted from finely ground tissue using TRI reagent at a ratio of 1 mL solution per 100 mg ground tissue (Sigma-Aldrich, #T9424-200ML). Residual phenol was removed from the crude extract through two chloroform extractions at a ratio of 1:5 v/v, followed by precipitation using isopropanol at 1:1 v/v. Precipitated RNA was washed twice with 70% ethanol and resuspended in a 1 mM sodium citrate buffer (pH 5.4). RNA quantification was performed through spectrophotometric analysis at 260 nm using the Nanodrop ND-1000 Spectrophotometer and RNA quality was assessed using 1% agarose gel electrophoresis or on the LabChip GX Touch (PerkinElmer). 5 µg of purified total RNA was combined with 5 µL of TURBO DNase buffer and 1 µL TURBO DNase (Thermo Fisher Scientific) in a 50 µL reaction, and incubated at 37°C for 30 minutes. DNA nuclease-treated RNA was then purified using 1.8X Sera-Mag paramagnetic particles.

qRT-PCR analysis

DNA nuclease-treated RNA was reverse transcribed into cDNA using either Invitrogen Superscript III (Thermo Fisher Scientific) or Maxima H Minus (Thermo Fisher Scientific) reverse transcriptase according to the manufacturer's instructions. For detection of mRNAs, 1 µg of DNA nuclease-treated RNA was combined with dNTPs and an Oligo$(dT)_{18}$ primer in a 4.5 µL reaction volume to final concentrations of 2.2 mM and 11.1 µM, respectively, and incubated for 5 mins at 65°C. For Superscript III based reverse transcription, 1x first strand reaction buffer, 10 mM DTT and 100 units of Superscript III Reverse Transcriptase was added to a final volume of 10 µL before incubation at 50°C for 60 minutes and 70°C for 15 minutes. For Maxima H Minus based reverse transcription, 1x reverse transcription buffer and 100 units Maxima H Minus Reverse Transcriptase was added to the reaction mix before incubation at 50°C for 30 minutes and 80°C for 5 minutes. For the detection of pre-mRNA, 500 ng of DNA nuclease-treated RNA was combined with 1.05 mM dNTPs and 10.5 µM random hexamers (Qiagen) in a reaction volume of 14.25 µL before incubation at 65°C for 5 minutes. 1x first strand reaction buffer, 5 mmol L=1 DTT and 150 U Superscript III (Thermo Fisher Scientific) were added to a final volume of 14.25 µL, before incubation at 25°C for 10 minutes, 50°C for one hour, and 70°C for 15 minutes.

Expression of mRNA and pre-mRNA was then assayed by semi-quantitative reverse-transcription PCR (qRT-PCR) on a Roche LightCycler480 using SYBR Green I (Roche Diagnostics). Raw fluorescence data were analysed using LinRegPCR to perform background subtraction, determine PCR efficiency, and calculate starting concentration [N_0; arbitrary fluorescence units (Ruijter et al. 2009; Ramakers et al. 2003)]. N_0 values were used to calculate fold-changes for target genes, which were normalised to changes in the housekeeper *PROTEIN PHOSPHATASE 2A SUBUNIT A3* (*PP2AA3*, *AT1G13320*). At least three biological replicates per genotype per time point were sampled, and each qPCR reaction was run in technical duplicate or triplicate. Primer sequences are provided in Supplementary Table 1.

mRNA sequencing

The Illumina TruSeq Stranded mRNA kit was used to prepare strand-specific (reverse-stranded: first read maps to the reverse strand) polyA-enriched sequencing libraries according to the manufacturer's instructions, except that all reactions were scaled-down by one-third and SuperScript III (Invitrogen) was used for first strand synthesis at 50 °C. Libraries were constructed using Illumina unique dual index adapters in a 15 cycle indexing PCR. All clean-up steps were performed using nuclease-free AMPure XP beads (Beckman Coulter) or Sera-mag SpeedBeads (GE Healthcare). Library concentration and fragment distribution were determined on the Qubit (double-stranded DNA high sensitivity kit, Invitrogen) and LabChip GX-Touch (DNA High Sensitivity kit, PerkinElmer), respectively. The concentration and peak fragment size were used to determine individual library molarity (assuming the average molar mass of one

DNA bp = 650 g/mol). Individual libraries were pooled in equal molar ratios and sequenced on a NextSeq500 (75 bp single-end, Supplementary table 2) at the ACRF Biomolecular Research Facility (Australian National University).

Raw sequencing reads were trimmed to remove adapter sequences and low-quality base calls (PHRED < 20, -q 20) with *Trim Galore!* (v0.6.4), a wrapper for *Cutadapt* (v1.18), followed by inspection with *FastQC* (v0.11.8). Trimmed reads were used for transcript quantification using *Kallisto* (Bray et al. 2016). *Kallisto index* (-k 21) was used to build a transcript index based on TAIR10 coding sequences [Ensembl release 51: Arabidopsis_thaliana.TAIR10.cdna.all.fa.gz (Kersey et al. 2016)]. Bootstrapped transcript-level abundances were computed using *Kallisto quant* (--rf-stranded --bias --single -b 10 -l 300 -s 100). Transcript-level abundance estimates were summarised to gene-level counts, using *Tximport* ['lengthScaledTPM' (Soneson et al. 2015)], for genes detected at an abundance of at least 0.5 TPM in more than six t_{10} samples (17,256 loci, Supplementary table 3). Rounded counts were input to *RUVSeq* in order to 'remove unwanted variance' associated with experimental batches using the *RUVr* workflow, except without performing global scaling (Risso et al. 2014). Differential gene expression analysis was performed on adjusted counts using the *edgeR* quasi-likelihood pipeline without TMM normalisation (Chen et al. 2016). A quasi-likelihood negative binomial generalised log-linear model was fit to the adjusted counts (glmQLFit, robust=T) followed by application of quasi-likelihood F-tests (glmQLFTest), with FDR correction for multiple hypothesis testing, to detect significant differentially expressed genes (FDR adjusted p-value < 0.05).

Adjusted counts were converted to abundance (counts per million, CPM) and used to compute fractional decreases in mRNA abundance (relative to the mean at t_{10} per condition). The t_{10} time point was shared between HL and REC samples as the same batch of infiltrated plants were either retained under HL or transferred to standard growth conditions for REC. Decay factor normalisation was performed to account for the apparent increase in abundance of relatively stable genes, which constitute a greater proportion of the total RNA pool while those less stable degrade without replacement during transcriptional inhibition (Sorenson et al. 2018). To do this, a decay factor was computed for each time point per condition, across the cordycepin-treated samples, using a set of highly abundant and stable reference genes. Reference genes were selected based on their abundance [>95th percentile ($\log_2$ CPM+0.01)] and variance [<25th percentile (coefficient of variation CPM)] across mock-infiltrated samples. This produced the following 52 reference genes: *AT4G01050, AT4G24280, AT5G36790, AT1G07920, AT5G13650, AT1G05850, AT1G62750, AT4G22890, AT3G62030, AT3G19170, AT2G18960, AT3G23400, AT5G42270, AT3G63140, AT3G11630, AT4G24770, AT1G65960, AT3G54050, AT4G01150, AT5G61410, AT1G11860, AT4G32260, AT5G60600, AT5G42980, AT3G55800, AT3G46780, AT3G16140, AT4G20360, AT3G14420, AT1G56070, AT5G66190, AT3G02470, AT1G30380, AT4G03280, AT2G30950, AT5G60390, AT4G04640, AT1G55670, AT3G60750, AT1G44575, AT5G35630, AT4G28750, AT1G20020, AT3G12780, AT5G50920, AT1G42970, AT1G20340, AT4G38970, AT4G37930, AT4G12800, AT5G01530, AT3G61470*. The mean fold-increase computed across reference genes in cordycepin-infiltrated samples should reflect the fold-change in the total RNA pool, thus providing a scaling factor that was applied on fractional decreases at each time point per condition. Lastly, any genes still displaying a fold-increase ≥1.5 after t_{10} were excluded from half-life analysis leaving 14,386 and 9,339 loci for unstressed and all conditions, respectively.

RNA half-life analysis

Decay factor normalised fractional decreases in mRNA abundance were used to compute half-life ($t_{1/2}$) per condition (assuming exponential decay and first order kinetics) (Ross 1995). The decay constant (k_d) was first computed using log-linear modelling of the change in mRNA abundance as a function of time using individual data points from cordycepin-infiltrated samples in each condition: $k_d = -\log_e[C/C_{10}]/dT$. From this, the condition-specific half-life of each gene could be solved using: $t_{1/2} = \log_e(2)/k_d$. The *R* package *lme4* was used for building linear mixed-effects models with fixed (Time) and random variables (experimental batch) (Bates et al. 2015). The conditional R^2 and accompanying F-statistic and p-value were used to evaluate whether the data fit an exponential decay model (p-value < 0.05) on a gene-by-gene basis, with the *R* packages *piecewiseSEM* and *lmerTest* (Lefcheck 2016; Kuznetsova et al. 2017). Finally, any genes calculated with $k_d < 0$ or half-life > 1,440 min (1 day) were removed from the analysis. In total, 6,711 and

3,960 genes could be reliably modelled under unstressed and all conditions, respectively. Half-lives calculated under unstressed conditions were directly compared to those reported for a common set of 4,497 genes across multiple genome-wide studies in Arabidopsis (Szabo et al. 2020; Sorenson et al. 2018; Narsai et al. 2007; Chantarachot et al. 2020). The R package *dabestr* was used to compute paired effect size parameters: paired mean difference (θ), paired median difference ($\mu_{1/2}$), and paired Cliff's delta (**δ**) using the functions *mean_diff*, *median_diff*, and *cliffs_delta*, respectively, with 10,000 bootstrap resamples. Functional enrichment tests were conducted using *ShinyGO* (FDR < 0.05), using all detected genes as background (Ge et al. 2020).

Polysome-associated mRNA sequencing

Polysome-associated mRNA sequencing was performed using an adapted protocol (Lecampion et al. 2016). Briefly, 250 mg of ground plant tissue was dissolved in 1 mL of polysome extraction buffer [160 mM Tris-Cl (pH 7.6), 80 mM KCl, 5 mM $MgCl_2$, 5.36 mM EGTA (pH 8), 0.5% IGEPAL CA-630, 40 U/mL RNasin Plus RNase inhibitor (Promega), 150 µg/mL cycloheximide, and 150 µg/mL chloramphenicol] and incubated on ice for 10 minutes. Samples were repeatedly centrifuged at 16,000 rcf for 5 minutes at 4°C until the supernatant was clear. Samples were loaded onto sucrose gradients, consisting of layers of 50% (1.68 mL), 35% (3.32 mL), 20% (3.32 mL) and 20% (1.68 mL), with the two 20% layers added separately (Lecampion et al. 2016). The buffer used in the gradients consisted of 400 mM Tris-Cl (pH 8.4), 200 mM KCl, 100 mM $MgCl_2$, 10.12 µg/mL cycloheximide and 10.12 µg/mL chloramphenicol. Gradients were centrifuged at 41,000 rpm with an SW41Ti rotor for 2 hours at 4°C. Each gradient was passed through a spectrophotometer from highest to lowest density and absorbance at 260 nm recorded, with 1 mL fractions collected. Fractions were pooled into monosomal and polysome sets and extracted using 5:1 acid phenol:chloroform. Briefy, an equal volume of the phenol:chloroform mix was added to each fraction, before centrifugation at 16,000 rcf for 10 minutes. The aqueous layer was extracted a second time using a one-fifth volume of chloroform, before the RNA was precipitated using an equal volume of isopropanol in addition to sodium acetate (pH 5.2) to a final concentration of 300 mM. The precipitated RNA was washed twice with 70% ethanol and resuspended in 1 mM sodium citrate (pH 5.4). Purified polysome RNA, and total mRNA purified from paired ground tissue (purified as described above), were used to generate sequencing libraries using the Illumina TruSeq Stranded mRNA kit as described above.

Quality control of raw reads was carried out using *FastQC*, with adapter trimming performed using *scythe* (-p 0.1) and quality trimming performed using *sickle* (-q 20 -l 20). Reads were aligned to the TAIR10 Arabidopsis genome using *subjunc* to report a single unambiguous mapping location per read (Liao et al. 2013). Sorting, indexing, and compression was carried out with samtools (Li et al. 2009) and read counts per loci were calculated using *featureCounts* [-s 2 for reverse stranded libraries, (Liao et al. 2014)]. Reads mapping to rRNA were removed before performing TMM normalisation and differential gene expression analysis, and calculating reads per kilobase of transcript per million mapped reads (RPKM) at the gene-level in *edgeR* (Robinson et al. 2010). Relative polysome loading (RPL) was calculated by dividing the RPKM of polysome-bound RNA by that of total RNA on a per replicate basis.

Data availability

All code used for analyses are available at GitHub (https://bit.ly/3yxp1XL). All sequencing data generated for this study are accessible at the NCBI's Gene Expression Omnibus (Edgar et al. 2002) through GEO Series accession numbers GSE201015 (https://www.ncbi.nlm.nih.gov/geo/query/acc.cgi?acc=GSE201015).

Results

Transcript-specific changes in transcription are evident during light stress and recovery

To determine whether changes in transcription might contribute to RRGD, we quantified levels of pre-mRNA, relative to mRNA, during 60 minutes of high light followed by 30 minutes of recovery for the RRGD loci *HSP101* (*AT1G74310*), *ROF1* (*AT3G25230*), and *GOLS1* (*AT2G47180*) (Figure S1 A-C). In general, changes in pre-mRNA mirrored those in mature mRNA during HL and REC. However, for both *HSP101* and *ROF1*, pre-mRNA levels during REC dropped below pre-stress levels, indicating a major decrease in mRNA production. During the same period, mRNA levels remained elevated over pre-stress levels by 4-fold (*ROF1*) and 8-fold (*HSP101*). In contrast, *GOLS1* pre-mRNA levels followed mRNA levels more closely during REC and never dropped below pre-stress levels, despite mRNA levels dropping even more rapidly than in *HSP101* and *ROF1*. For all three genes, pre-mRNA levels remained above pre-stress levels in samples that experienced HL beyond 60 minutes, indicating ongoing transcription. These results suggest that transcriptional changes contribute towards RRGD, likely in a transcript-specific manner.

Syringe-infiltration of cordycepin effectively inhibits transcription in mature leaves

We first sought to quantify *in planta* mRNA half-lives in mature soil-grown plants during stress and recovery. Quantification of mRNA half-life is typically performed with juvenile seedlings grown on nutrient-rich media, or cell culture (Chantarachot et al. 2020; Sorenson et al. 2018; Szabo et al. 2020; Narsai et al. 2007). While these systems allow for effective administration of transcriptional inhibitors (e.g. cordycepin or actinomycin D) or uridine analogs for pulse labelling, they do not allow for studies in mature soil-grown plants alongside applications of external stimuli (e.g. abiotic stress). Therefore, it is currently unclear whether existing measurements of RNA half-lives are reflective of mature soil-grown plants. To address these limitations, we developed a method of administering cordycepin that allowed the simultaneous application of stress treatments. Syringe-infiltration was considered a viable procedure for administering cordycepin into the cells of mature Arabidopsis leaves, which presented two advantages. First, it allowed for *in situ* treatment of soil-grown plants during light stress. Second, since the treatment was applied to individual leaves, a mock treatment could be applied to a separate leaf on the same plant as a control.

We first evaluated the ability to achieve effective transcriptional inhibition using syringe-infiltration into individual leaves for 10 minutes before exposure to light stress (Figure 1 A-B). Induction of light-responsive genes was then evaluated using qRT-PCR. While strong induction of *HSP101* and *HSP17.4B* was observed when infiltrated with a mock buffer, a dramatic reduction in their induction was observed when infiltrated with cordycepin. For example, *HSP101*, which was up-regulated 375-fold after 30 minutes of high light in mock-treated leaves, was only elevated 4.5-fold in the presence of cordycepin. This equated to a 98.8% reduction. A similar block of induction was observed for *HSP17.4B*. We next examined how long the cordycepin remained effective after infiltration; an important consideration for RNA half-life measurements over 60 minutes. Plants were infiltrated with cordycepin and then incubated for 10, 30 or 60, under US conditions, before exposure to stress, with efficacy measured via induction of *HSP101* (Figure 1 C). Relative to the 375-fold induction in the absence of cordycepin, the highest induction achieved was only 12-fold when cordycepin was applied. Therefore, cordycepin delivered via syringe infiltration was considered effective over a 60 minute time frame. However, it was uncertain whether the application of cordycepin to one leaf could cause systemic effects, which would affect the ability to mock infiltrate a separate leaf on the same plant as an internal control. To test this, individual plants were subject to either mock infiltration (M) or mock and cordycepin infiltration (M+C), followed by 15 minutes of light stress, and compared to an untreated control (U). In addition to harvesting the infiltrated leaves, an non-infiltrated leaf was also taken from each plant for comparison (Figure 1 D). For non-infiltrated leaves, no significant difference in *HSP101* induction was observed between treatment regimes (ANOVA, $P = 0.216$), nor for mock treated leaves (unpaired Student's t-test, $P = 0.633$). In both cases, small increases in mean expression was observed as the number of infiltrated leaves per plant increased. While not statistically significant, this suggested that the infiltration itself could stimulate stress-responsive genes. Critically, it was

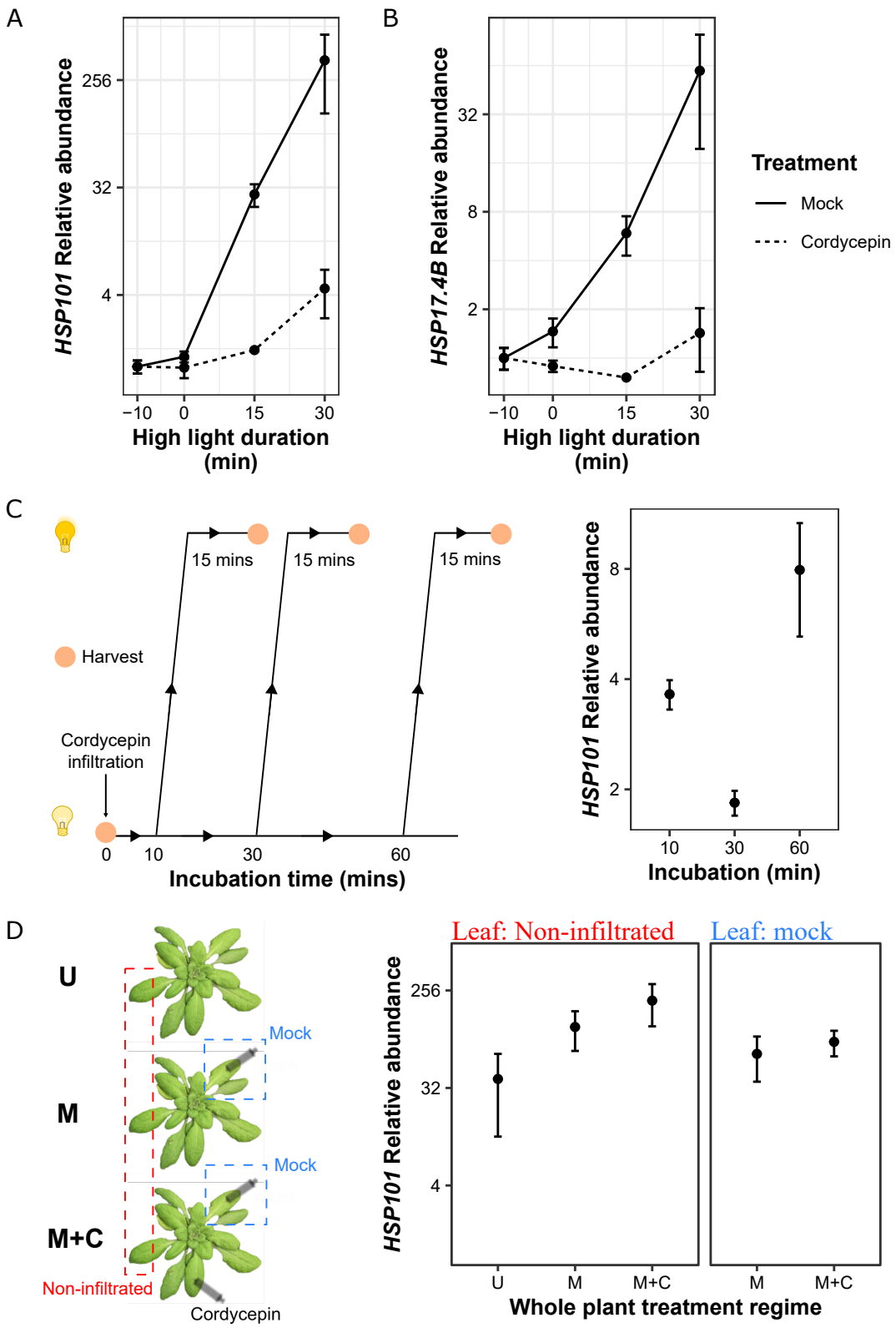

Figure 1. Syringe infiltration of cordycepin inhibits high-light induced transcription without systemic effects

(A-B) High light induction of *HSP101* and *HSP17.4B* was measured over 30 minutes folowing infiltration of individual leaves with mock or cordycepin solution. Points denote means, error bars denote standard error of the mean (n=2).

(C) Arabidopsis plants were syringe-infiltrated with cordycepin and then incubated for 10, 30, and 60 minutes before exposure to 15 minutes of high light.

(D) Arabidopsis plants were subject to three different infiltration regimes: untreated (U), mock infiltration (M), or mock and cordycepin infiltration (M+C). Treatment was followed by 15 minutes of light stress prior to sampling untreated and mock infiltrated leaves. Points denote means, error bars denote standard error of the mean (n=3).

clear that transcriptional inhibition following application of cordycepin did not impair the induction of genes in distal untreated or mock-infiltrated leaves. Taken together, we concluded that syringe-infiltration presented an effective means to administer cordycepin to Arabidopsis leaves.

Feedback regulation of mRNA stability in mature Arabidopsis leaves

With a functional cordycepin assay established for use under high light, a time course experiment was conducted to estimate RNA decay rates in US, HL, and REC conditions (Figure 2 A). In each instance, infiltration of mock or cordycepin solution was followed by at least three harvesting time points at 10 minute intervals. Infiltration of the two solutions was performed on independent leaves from the same plant to minimise biological variation between treatments, followed by mRNA sequencing. To examine whether syringe-infiltration of cordycepin led to widespread transcriptional inhibition, differential gene expression was assessed between the first and last time points following cordycepin and mock infiltration (Figure S2 A). For mock-treated samples, no particular bias toward up- or down-regulation was observed; by contrast, cordycepin treatment caused strong down-regulation in each condition. For example, during recovery 5,178 genes were down-regulated following cordycepin infiltration, while just 584 genes were upregulated. The up-regulation likely represents relatively stable transcripts that become comparatively more abundant as the RNA pool shrinks, leading to the appearance of increased expression. Furthermore, the magnitude of down-regulation was greater following cordycepin treatment compared to mock. Notably, 826 genes were differentially expressed after mock treatment in US conditions, indicating that the infiltration itself may be affecting substantial changes on the transcriptome independent of cordycepin treatment. Nonetheless, this data confirms that widespread transcriptional inhibition was achieved in mature Arabidopsis leaves using syringe-infiltration of cordycepin.

We next sought to compute mRNA half-lives across the transcriptome in unstressed Arabidopsis. Current measurements of mRNA half-lives in Arabidopsis are determined using tissue culture with actinomycin D treatment (Narsai et al. 2007), or nutrient-rich media-grown juvenile seedlings using uridine analogs (Szabo et al. 2020) or cordycepin treatment (Sorenson et al. 2018; Chantarachot et al. 2020). We compared whether mRNA half-life in these systems were comparable to observations in mature soil-grown Arabidopsis leaf tissue. Log-linear regression was performed using normalised fractional decreases of mRNA abundance in cordycepin-infiltrated samples to compute k_d, which allows for calculating mRNA half-life that was used for comparisons. From the unstressed samples, half-lives could be computed for 6,711 genes based on statistical appropriateness of the fitted regression (Supplementary table 4, $p < 0.05$). The relatively small number of transcripts for which half-lives could be computed is likely the result for the reduced number of time points, short timescales, and infiltration induced expression. Half-lives were extracted from the aforementioned studies for which 4,497 genes could be directly compared (Figure 2 B). Indeed, the mRNA half-lives observed in this study had a median of 24.1 mins, which is substantially lower than the prior studies with median 79.2 - 157.6 mins. This was further supported by computing bootstrapped effect size parameters (mean difference, θ; median difference, $\mu_{1/2}$, Cliff's delta, $\boldsymbol{\delta}$) (Table 1). In particular, the bootstrapped median difference in mRNA half-lives between datasets varied between 52 - 131 mins, with corresponding Cliff's delta in the range of 0.81 - 0.95 (where a positive value represents the likelihood of observing a larger value). Larger values were observed when computing mean differences between datasets, likely caused by a small number of transcripts that displayed very large half-lives in some datasets.

Next, we explored which transcripts exhibited reduced stability in mature Arabidopsis leaves and their biological roles. To define transcripts with lower stability, we compared half-lives obtained here with each published dataset on a gene-by-gene basis. Those with lower half-lives, by a difference greater than the median difference, compared to each dataset were collated (Figure 2 C). There were 1,471 transcripts with lower stability than in at least three of the existing datasets. These had striking enrichments of GO terms relating to post-transcriptional and translational processes (Figure 2 D), such as RNA processing, ribosome biogenesis, RNA and tRNA binding, and RNA catalysis (including pyrophosphatase and nucleoside triphosphatase activity). This suggests the occurrence of feedback regulation of RNA processing, splicing, and translation through altered mRNA stability in mature Arabidopsis leaves.

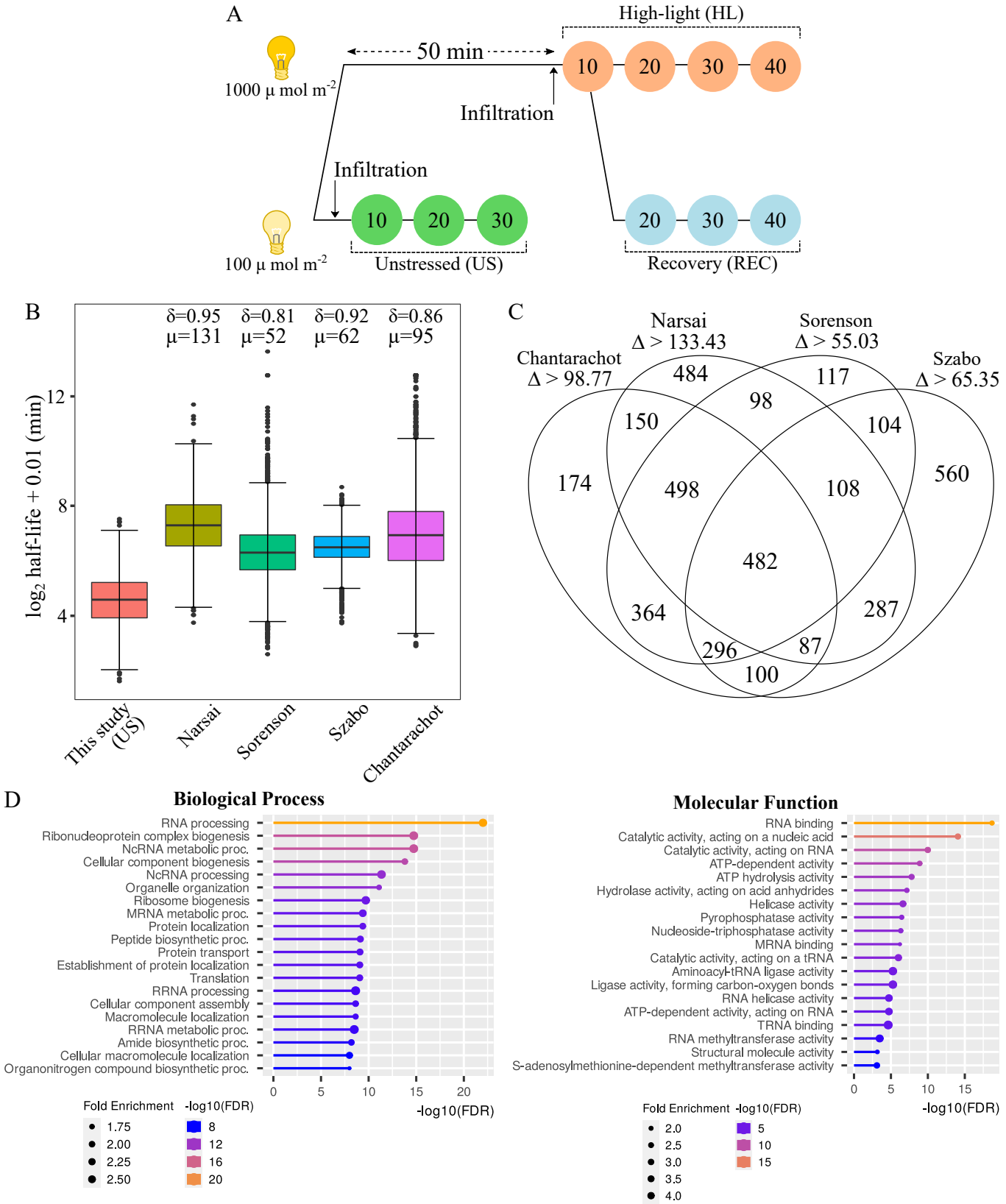

Figure 2. Sampling strategy to determine mRNA half-lives in Arabidopsis leaves
(A) Unstressed plants were harvested in standard growth conditions (US, 100 µmol m^{-2} s^{-1}) at three time points in ten minutre intervals post-infiltration. High light and recovery plants were exposed to 60 minutes light stress (HL, 1000 µmol m^{-2} s^{-1}), with infiltration occurring at 50 minutes. Following harvesting at 10 minutes post-infiltration (60 minutes HL), plants were either kept under HL or moved for recovery (REC, 100 µmol m^{-2} s^{-1}) for three harvesting points at ten minute intervals.
(B) Boxplots depicting log_2 half-life determined for 4,497 genes under US conditions here, and their corresponding values from other studies. Box denotes median and interquartile range, bars denote 1.5xinterquartile range, and points denote outliers. δ denotes Cliff's delta (the likelihood of observing a difference between groups) compared to this study. µ denotes the computed median difference compared to this study.
(C) Venn diagrams representing the number of genes exhibiting a decreases in half-life greater than the median difference for each dataset compared to this study.
(D) Top enriched GO terms for products of transcripts with reduced half-life in mature Arabidopsis leaves.

Dynamics of mRNA stability during light stress and recovery

Profiling RNA abundance during HL and REC conditions revealed three broad patterns of decay that were observable across conditions, including transcripts undergoing relatively fast, moderate, or slow decay (Figure 3 A, Supplementary table 5). Transcript abundance appeared to decline to a greater magnitude under HL, suggesting that mRNAs were being destabilised. Curiously, there was a transient increase in abundance 20 minutes post-infiltration during REC, particularly in slow decaying transcripts. It is unclear whether this reflects residual transcription or is the result of these slow decaying transcripts occupying a greater portion of the RNA pool as others are degraded. To quantify this destabilisation, we computed mRNA half-lives, for 3,960 genes that could be reliably modelled ($p < 0.05$), under US (Med $t_{1/2}$ = 20.8 mins), HL (Med $t_{1/2}$ = 15.1 mins), and REC (Med $t_{1/2}$ = 19.8 mins, Figure 3B). While the bootstrapped median difference was only -1 min (δ = -0.03) between US and REC, a difference of -4.21 min (δ = -0.27) was observed under HL. This suggests that there is a bias towards destabilisation of transcripts under HL, which are re-stabilised during REC. We tested whether our RNA half-life analysis was biased towards low abundance transcripts, which may be more prone to destabilisation. However, it was clear that the 3,960 transcripts captured in our analysis were of widely varying abundance (Figure S2 B). Comparing the half-life ratio under HL ($t_{1/2}$ HL : $t_{1/2}$ US) with the fold-change in mRNA abundance revealed a negligible relationship (Figure 3 C). However, there appeared to be a subset of highly induced transcripts that were destabilised and another portion of down-regulated transcripts that underwent stabilisation. Of the 388 RRGD loci defined previously (Crisp et al. 2017), 70 were captured in this RNA half-life analysis. As expected, these were predominantly up-regulated (64/70 = 91.4%) when contrasted between HL and US mock-treated leaves (10 minutes post-infiltration). Indeed, these 64 genes comprised the majority of the most highly up-regulated genes by HL. Within this up-regulated subset, there was a clear bias towards destabilisation (55 / 64 = 85.9%), which suggests a coupling between increased abundance and destabilisation.

Exploring the 1,980 transcripts with a reduction in half-life greater than the median difference, revealed enrichment for transcriptional processes, such as chromosome and chromatin organisation, DNA and histone binding activity, and (DNA) helicase activity (Figure 3 D). Paired with this were terms related to the regulation of broad metabolic and biosynthetic processes, as well as post-embryonic development and reproduction. Once more, feedback regulation was observed, albeit to a lesser extent, with enrichments in mRNA metabolism and RNA helicase activity. Therefore, light stress appears to induce the destabilisation of transcripts involved in both transcriptional and post-transcriptional regulation, as well as the transition towards reproductive growth.

Since it appeared that destabilisation of transcripts occurred under HL, we investigated the timing of this destabilisation. To test this, plants were exposed to high light for 60 minutes, with subsets of plants infiltrated with mock or cordycepin solution at 5, 20 and 50 minutes. Samples were then harvested at 10, 20 and 30 minutes post-infiltration to measure decay rates using qRT-PCR of *AT3G14200*, which exhibited HL-induced destabilisation (Figure S3 A). Plants infiltrated at 5 minutes HL exhibited an increase in *AT3G14200* in the 10 minutes following infiltration, which may be attributed to residual transcription while the cordycepin took effect; however, transcript levels did decline from 10 to 30 minutes post-infiltration. In both the 20 minute and 50 minute treatment groups, steeper and more consistent declines were observed in the 30 minutes post-infiltration. To quantify these differences, RNA half-life was modelled using the period 10 to 30 minutes post-infiltration. The half-life of *AT3G14200* after 5 minutes HL was estimated at 35.58 minutes, but this model was not significant (P_{adj} = 0.149). By contrast, the half-lives following infiltration at 20 and 50 minutes HL were estimated at 19.91 and 16.45 minutes, respectively (P_{adj} = 0.00027). This indicated that *AT3G14200* transcripts were more stable during the initial period of high light stress and were subsequently destabilised.

The finding that *AT3G14200* is destabilised based on the duration of stress suggests that RRGD, typically observed after 60 minutes, may not occur with shorter durations of HL. To test this, plants were exposed to 10, 30, 60 and 120 minutes HL before being moved to REC (Figure S3 B-D). Quantification of relative changes in canonical RRGD loci: *HSP101*, *ROF1*, and *GOLS1* using qRT-PCR revealed that 10 minutes HL did not cause recovery-induced down-regulation. By contrast, clear declines in transcript levels were observed when moved to REC at 30 and 60 minutes HL, while a small increase was observed

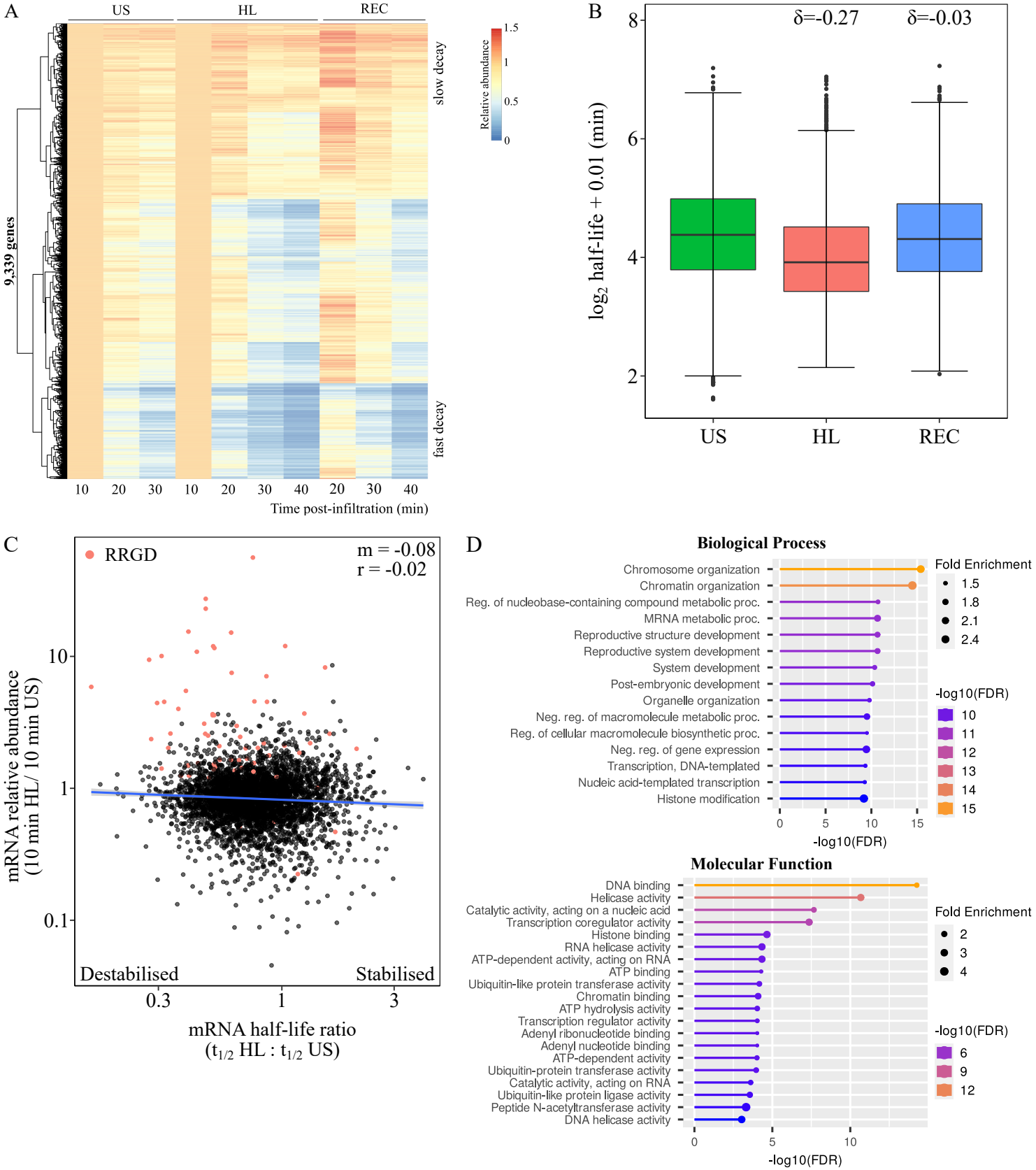

Figure 3. Subtle destablisation of mRNAs during HL

(A) Heatmap with 1-dimensional hierarchical clustering depicting relative abundance of 9,339 genes in cordycepin-infiltrated samples under US, HL, and REC conditions.

(B) Boxplots depicting $\log_2$ half-life determined for 3,960 genes under US, HL, and REC conditions. Box denotes median and interquartile range, bars denote 1.5 x interquartile range, and points denote outliers. δ denotes Cliff's delta.

(C) Scatter plot presenting the fold-change in mRNA abundance (10 min HL/10 min US), in mock treated-samples, versus the half-life ratio (HL/US) for 3,960 modelled transcripts. Points represent individual genes, line denotes fitted linear model, 'm' denotes regression coefficient, and 'r' denotes Pearson's correlation coefficient.

(D) Top enriched GO terms for products of transcripts destablised under HL.

followed by a decline after 120 minutes. Gene expression patterns seen in *GOLS1* were similar, though declines in transcript levels were observed in the last 10 minutes of REC after each HL length. Estimations of RNA half-lives were modelled for each REC period, however, following adjustments for multiple comparisons no model was significant ($p < 0.05$). Nonetheless, they did indicate the same general trend, with the most notable down-regulation being observed following 60 minutes HL. This data reinforced the cordycepin data obtained for *AT3G14200* and indicated that RRGD loci remain comparatively stable in the early stages of HL before being destabilised.

Translational regulation occurs during late stress and early recovery

To investigate the interplay between mRNA stability and translation during HL and REC, we sequenced polyribosome (polysome)-bound mRNAs, which are being actively translated. This was done after 30 and 60 mins HL, and 7.5, 15, and 30 minutes REC (Supplementary table 6). During polysome fractionation, we produced a spectral profile to identify specific fractions and test for shifts in the translational landscape (Figure S4). Indeed, we were able to distinguish monosomes from polysome fractions, which separate based on the number of ribosomes bound to a transcript (Figure S4 A). The amount of RNA bound in each fraction was highly similar between samples, indicating little change in the transcripts loaded onto monosomes relative to polysomes (Figure S4 B). Although a major disruption was not observed, individual transcripts may still undergo substantial translational regulation. To examine this, we sequenced the total and polysome-bound mRNA populations and calculated fold-changes between time points on a per-gene basis, which were then compared between the two populations. Changes in total mRNA and polysome-bound mRNA were highly correlated (Pearson's $r = 0.81$) in the early stages of stress (0-30 minutes) indicating loading of transcripts onto polysomes proportional to changes in transcript abundance (Figure 4 A). However, during the later period of stress (30-60 minutes) the two populations were substantially less correlated (Pearson's $r = 0.47$). By 30 minutes REC, this correlation was restored (Pearson's $r = 0.77$). However, at early REC time points, the changes between the two populations were more weakly linked, particular during the first 7.5 minutes of REC (Pearson's $r = 0.25$, Figure S4 C). Such a decoupling of total and polysome-associated mRNA abundance during late stress and early REC indicates translational regulation on a subset of transcripts. Notably, this suggests that changes in translation are occurring independently of a concomitant change in total mRNA.

As ribosomes are recruited onto transcripts across the total cellular pool, it can be informative to examine the ratio between polysome-bound and total mRNA. Since ribosome density was not measured, this is not a reflection of translation efficiency. Therefore, to avoid confusion, we refer to this as relative polysome loading (RPL), where a value of one indicates that polysome-associated and total mRNA occur at proportionally the same abundance. It is important to note that changes in RPL can occur via differential recruitment of ribosomes to transcripts (numerator) or changes in total transcript abundance (denominator). Notably, RPL can increase even if levels of polysome-associated mRNA decrease provided this occurs at a slower rate than a reduction in total mRNA abundance. Therefore, comparing changes between RPL and total mRNA can be used to more easily identify shifts that occur in only one population. This comparison was performed for three periods: early HL (0-30 mins), late HL (30-60 mins) and REC (Figure 4 B). On a broad scale, clear differences could be observed between the three periods although a striking proportion of transcripts showed changes in RPL with no change in total mRNA (early: 13.22%, late: 22.87%, REC:10.9%). In each period, these changes were enriched for regulation in opposing directions with early HL and REC being biased towards reduced RPL whereas late HL showed a striking enrichment of genes with increased RPL. Such results indicate a bias toward translational repression after the onset of stress, followed by increased polysome loading. Notable too were the changes in the proportion of transcripts showing differences in RPL relative to total mRNA, reflecting differential polysome-association to transcript abundance. During early stress, 20.8 % and 19.2% of transcripts exhibited changes in RPL and total mRNA, respectively, a 1.1:1 ratio. During late stress, 25.9% and 7.7% of transcripts had changed RPL and total mRNA, respectively, a 3.4:1 ratio (3-fold increase). In recovery, this returned to 15.7% and 16.8% changes in RPL and total mRNA, respectively, reflecting a 0.9:1 ratio. Overall, these results highlight the extent of regulating translation during light stress and recovery, with late stress period (30-60 minutes HL)

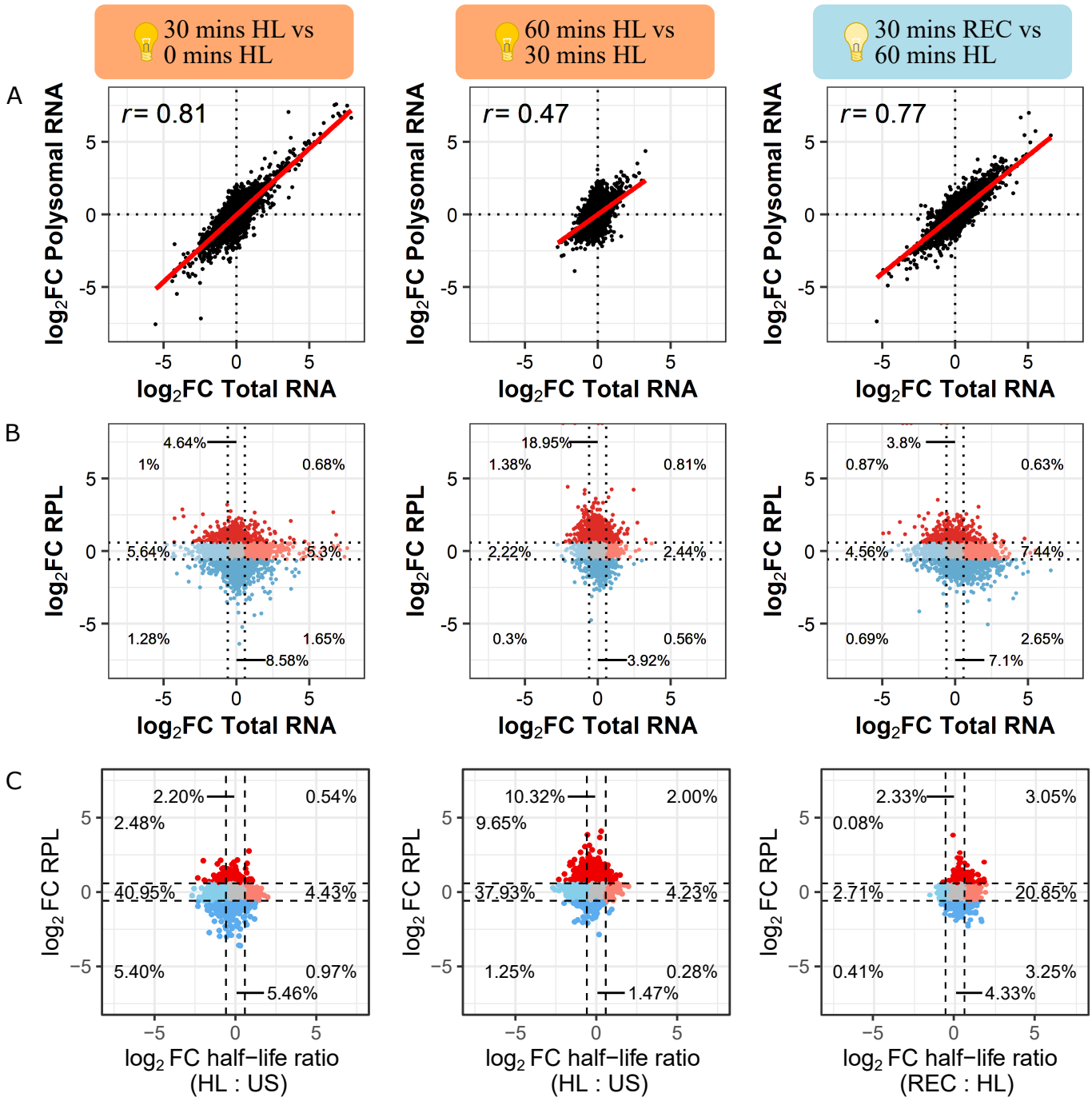

Figure 4 Translational regulation during light stress and recovery
(A) Scatter plots comparing fold-changes in total and polysome-bound mRNA populations between time points.
(B) Scatter plots comparing fold-changes in total mRNA and relative polysome loading (RPL = polysomal mRNA / total mRNA) between time-points.
(C) Scatter plots comparing fold-changes in RPL and half-life ratios between time-points. relating transcript half-life to their abundance in the polysome-bound mRNA fraction and RPL.
Colouring indicates fold change greater (red) or less (blue) than 1.5 for either total mRNA or RPL.
Numbers denote proportion of transcripts detected in each section. Points represent individual transcripts, line denotes fitted linear model, and 'r' denotes Pearson's correlation coefficient.

being a dynamic period for translation showing increased ribosome-loading of many transcripts independently of changes in total mRNA.

Since mRNA stability may influence translation, we examined the relationship between mRNA half-life and RPL during the same early HL, late HL, and REC periods. We hypothesised that destabilised transcripts would show reduced polysome-association. To do this, we related the fold-change in RPL, measured for each period, to the half-life ratio (i.e. the change in stability) observed under HL and REC for 3,905 genes detected in each dataset (Figure 4 C). There was no clear relationship between changes in RPL and mRNA stability. Under both periods of HL, there was a large proportion of transcripts that were destabilised yet had unchanged RPL indicating that the majority of destabilised transcripts retained similar levels of polysome recruitment. Conversely, during recovery there is a clear increase in the stability of many transcripts yet the majority of these also showed no difference in RPL. Taken together this suggests that changes in mRNA stability are not strongly linked with changes in polysome-association or dissociation.

Light-induced transcripts have increased polysome loading during late stress

We next investigated whether HL-induced genes demonstrated greater association with ribosomes. HL-induced genes were identified as those which exhibited at least a three-fold increase in mRNA abundance after 30 minutes HL. These were categorised based on their expression profiles: category 1 genes remained up-regulated through HL and REC, category 2 genes were down-regulated during REC, and category 3 genes were down-regulated after 30 minutes HL (Crisp et al. 2017). Examination of polysome-associated transcripts found that they exhibited an expression profile concordant with that observed in total mRNA (Figure S5). This suggests that the free and polysome-bound mRNA populations were tightly linked, and changes in mRNA abundance of a given gene generally led to a corresponding change in its translation. Furthermore, this indicates that the phenomenon of RRGD is likely to have tangible cellular consequences with respect to protein production.

Increased indices of co-translation decay were observed in RRGD loci, suggesting its involvement in clearing light-induced transcripts (Crisp et al. 2017). Therefore, it was hypothesised that a decrease in RPL, of RRGD loci, would be observed as their polysome-associated transcripts would be degraded at a higher rate than free mRNA. To test this, changes in RPL within the three 30 minute periods that made up the time course were compared between the three categories (Figure 5). Genes in categories 1 and 3 tended to have an increase in RPL during 30-60 minutes HL. This was particularly notable for category 3 transcripts that declined in the total mRNA pool, suggesting that this down-regulation was unlikely the result of co-translational decay. However, both these categories exhibited declines in RPL during REC, indicating either unloading of polysomes or degradation of polysome-associated transcripts by co-translational decay.

Discussion

To dynamically regulate gene expression during stress and recovery, plants can alter transcription, mRNA stability, and translation or a combination. Here, we characterise changes in each during high light and recovery, where we previously observed rapid temporal changes in mRNA abundance (Crisp et al. 2017). Our focus was the extent to which mRNA stability was modulated to control RNA abundance, and the subsequent impacts on translation. Changes in transcription were based on quantifying changes in pre-mRNA levels, which appeared to decrease upon perception of recovery. Meanwhile, mRNA destabilisation occurred during light stress followed by re-stabilisation during recovery. This destabilisation did not occur immediately, rather it occurred after 30 minutes of high light at which point light-induced genes reached peak expression. Similarly, recovery-induced down-regulation was not observed in plants exposed to a brief 5 minute stress, indicating that destabilisation is dependent on the duration of exposure. Further, we find that light induced transcripts showed concordant changes in polysome loading as total mRNA levels. Based on our findings, we propose the following model of mRNA dynamics during light stress and recovery (Figure 6). Onset of stress is associated with a burst of light-induced transcription, which occurs for 30 minutes. Following this, mRNA stability decreases and transcription slows, leading to slower accumulation in overall abundance. Yet, preferential loading of specific transcripts occurs during late stress. Upon

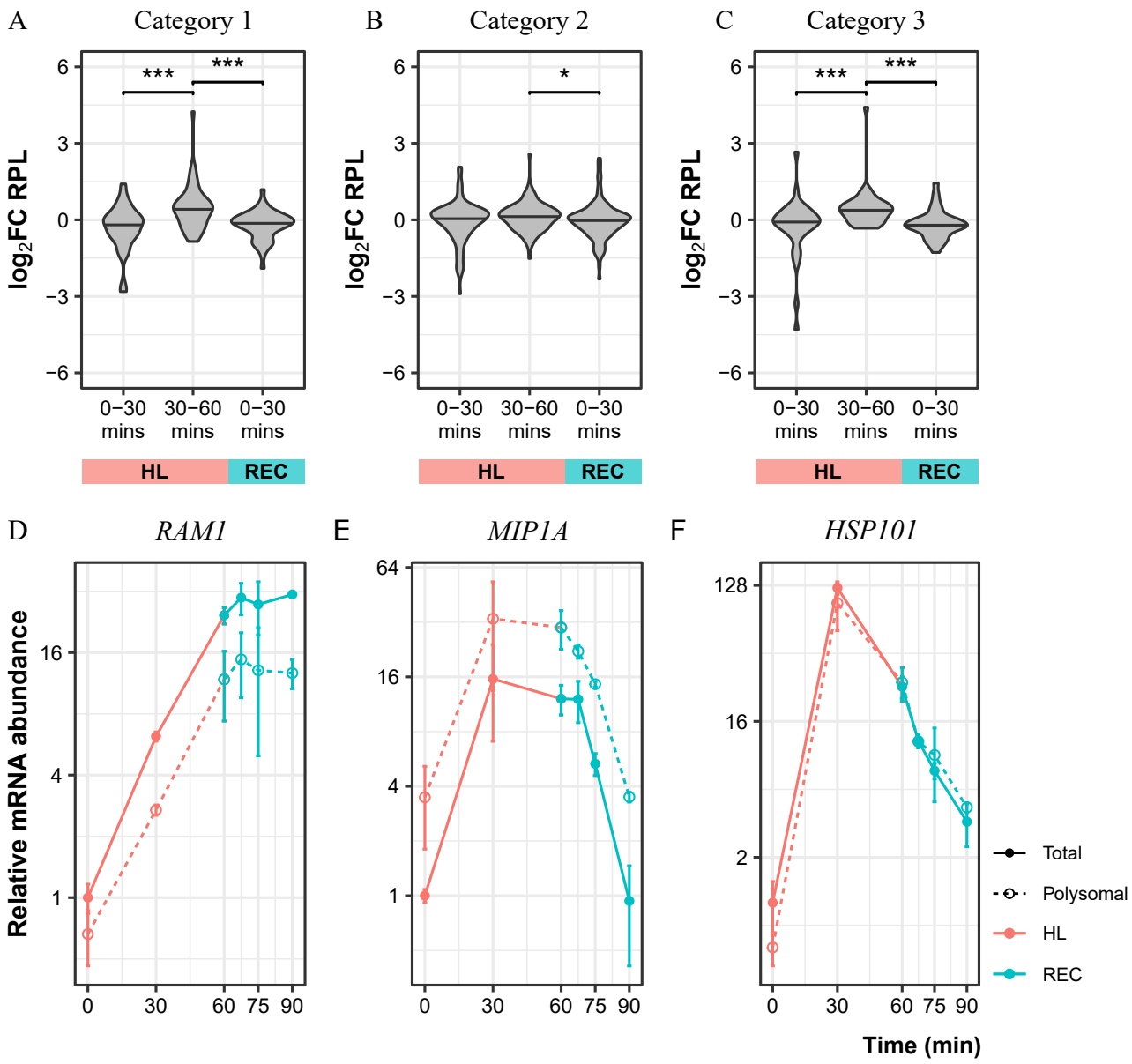

Figure 5 Light-induced transcripts exhibit elevated ribosome-association during late stress
(A-C) Light-induced genes were divided into categories based on expression profiles during late stress and recovery. Changes in RPL were compared across the three 30 minute time periods and are represented as violin plots. Median fold-change was compared using Wilcoxon Rank-sum test, * denotes $P < 0.05$, *** denotes $P < 0.001$.
(D-F) Examples of gene expression profiles in each category. Points denote mean, error bars denote SE.

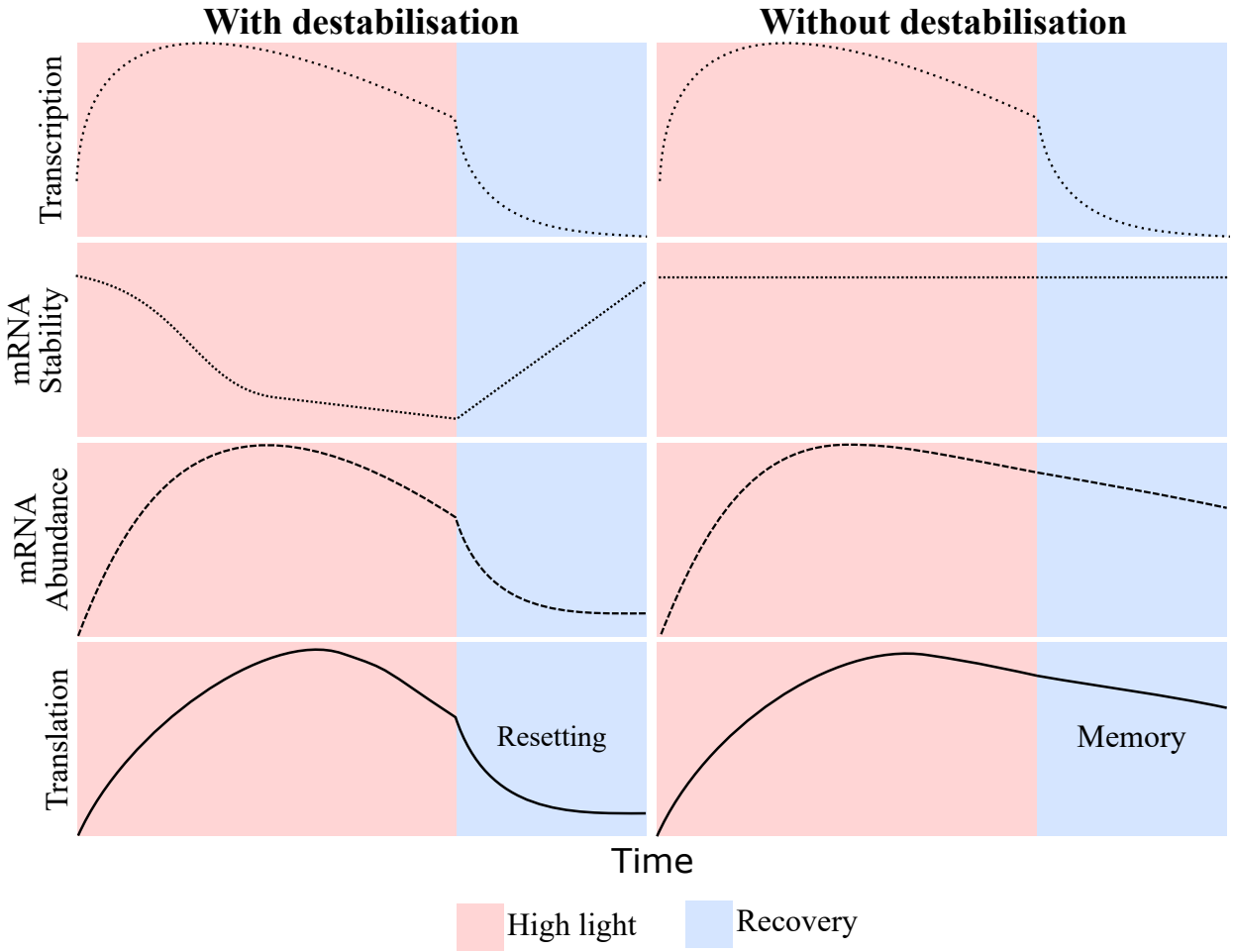

Figure 6 Stress-induced transcript destabilisation facilitates rapid recovery gene down-regulation
A proposed model of transcript dynamics during high-light and recovery. While transcription appears to rapidly decrease during recovery, the corresponding down-regulation in transcript abundance and resetting of the transcriptome is likely dependent on prior destabilisation. In its absence, transcript levels remain elevated during recovery, maintaining the stress response and potentially leading to stress memory.

entering recovery, transcription ceases, virtually shutting off for some genes. Due to the prior destabilisation of transcripts, a rapid down-regulation in overall, and polysome-associated, transcripts occurs, causing a resetting of the transcriptome to near pre-stress levels. In this way, changes in mRNA stability act as the necessary precursor to RRGD, maximising the impact of the transcriptional shut-off by accelerating transcript turnover during this period.

Dynamic mRNA stability during plant development and light stress

Half-lives of mRNA were measured in mature Arabidopsis leaves using a newly developed method, based on syringe-infiltration of cordycepin. This allowed us to test for differences in mRNA stability in older plants, since existing measures have been performed in juvenile seedlings. Indeed, we observed a substantial decrease in half-life for the majority of genes that could be contrasted with existing datasets (Szabo et al. 2020; Sorenson et al. 2018; Narsai et al. 2007; Chantarachot et al. 2020). Those transcripts exhibiting reduced stability in mature leaves were strongly enriched to encode proteins involved in post-transcriptional processes, including involvement in RNA processing and catalysis, RNA binding, ribosome biogenesis, and translation (Figure 2 D). This may reflect feedback regulation of post-transcriptional processes to tailor protein synthesis requirements. Contrary to a mature leaf, juvenile seedlings growing in nutrient-rich media will likely be undergoing higher rates of cell division (Donnelly et al. 1999; Dean and Leech 1982; Desvoyes et al. 2006) and chloroplast development (Pogson et al. 2015; Dean and Leech 1982). When paired with a ready supply of the requisite macromolecules, this is likely driving higher rates of protein synthesis and turnover (Li et al. 2017; Ishihara et al. 2015).

We previously hypothesised that mRNA stability was modulated during recovery based on observations of a rapid decline in the abundance of light-induced transcripts (Crisp et al. 2017). The use of syringe-infiltration allowed application of cordycepin *in situ* to plants undergoing stress and recovery. Contrary to expectations, we observed transcript destabilisation under high light followed by re-stabilisation upon recovery (Figure 3 B). Typically, half-life measurements are measured over a longer period over hours rather than 30 minutes as performed here. This has potentially biased our analysis to relatively unstable transcripts since longer time courses are needed to model statistically significant changes of more stable transcripts. We also observed a pronounced increase in the abundance of a subset of transcripts within 10 minutes of recovery (Figure 3 A, 20 minutes post-infiltration) as was documented previously (Crisp et al. 2017). This may reflect residual transcription occurring during late light stress as observed for three RRGD genes (Figure S1), unperturbed by 20 minutes of cordycepin infiltration. Nonetheless, our observations were made on 3,960 transcripts that could be reliably modelled in the three conditions tested and reveal transcript destabilisation occurring during light stress, which facilitates RRGD upon recovery, in Arabidopsis. The length of stress required for this destabilisation appears to be at least 20 minutes based on observations in RRGD loci: *AT3G14200*, *HSP101*, *ROF1*, and *GOLS1* (Figure S3). It remains to be investigated if this is a truly global response, beyond the 3,960 transcripts compared here, and whether the same duration is required for different types of stress.

The destabilisation of stress-induced transcripts has been observed more broadly including in yeast exposed to oxidative stress, using treatments of 25 minutes hydrogen peroxide (Shalem et al. 2008) and 6-30 minutes NaCl (Molin et al. 2009), and Arabidopsis cells undergoing 24 hours of cold stress (Chiba et al. 2013). That stress-responsive genes are destabilised during stress appears counterintuitive. However, this likely confers faster responsivity since unstable transcripts have shorter transition times in reaching new steady state levels (Ross 1995; Pérez-Ortín et al. 2007). Such an inverse relationship in which unstable transcripts are more quickly induced has been observed in multiple eukaryotes, in a gene- and stress-specific manner (Molina-Navarro et al. 2008; Elkon et al. 2010). While such a strategy is energetically costly, the benefits are faster responses to both the initial stress and perception of recovery (Shalem et al. 2008). This response is not necessarily global, as transcript-specific responses are also observed, likely influenced by the type and duration of the stress. For example, 15 minutes of osmotic shock in yeast led to widespread transcript destabilisation, while a small subset (121 genes, 2.2%) of stress-induced transcripts were preferentially stabilised (Romero-Santacreu et al. 2009). In contrast, the stabilisation of stress-induced transcripts was observed in yeast experiencing a slow enduring stress (40 minutes methyl methanesulfonate treatment) (Shalem et al. 2008). Similarly in Arabidopsis, longer term salt stress (2 weeks) was also associated with the stabilisation of salt-induced transcripts encoding stress-response

proteins, alongside increased N^6-methyladenosine deposition (Kramer et al. 2020; Anderson et al. 2018). This preferential stabilisation likely reflects the activity of mRNA-binding proteins controlling transcript localization. For example, SPI functions to relocalize its mRNA targets towards processing bodies for stabilisation during salt stress (Steffens et al. 2015).

Rapid recovery gene down-regulation occurs as a result of stress-dependent mRNA destabilisation and transcriptional shut-off

The rapid decline in transcript levels of RRGD loci upon recovery appears to be facilitated by the combination of destabilisation during stress and transcriptional shut-off upon recovery. Indeed, previously defined RRGD loci that are highly up-regulated during light-stress were among the most destabilised transcripts (Figure 3 C). We estimated transcriptional changes by detecting pre-mRNA through use of intronic primers amplifying segments of unspliced mRNA (Zeisel et al. 2011). Such changes are inferred under the assumption that the conversion of pre-mRNA to mRNA is constant, which could be disrupted by differential splicing or nuclear RNA decay. Unsurprisingly, changes in pre-mRNA levels tracked closely with those of mature mRNAs for the genes profiled (Figure S1). However, important differences were observed that likely reflect differential regulation of distinct light-responsive transcripts. From previous observations, *HSP101* and *ROF1* decline in abundance after 30 minutes of high light, whereas *GOLS1* declines specifically during recovery (Crisp et al. 2017). For *HSP101* and *ROF1*, pre-mRNA levels (and, by proxy, transcription) declines to below pre-stress levels during recovery, effectively ‘shutting-off’ transcription, while mRNA levels remain comparatively elevated. By contrast, *GOLS1* pre-mRNA levels more closely resembled those in mRNA, and did not decline to or below pre-stress levels during recovery. This likely reflects differing transcriptional repression of light-responsive transcripts during recovery, which could be further unpacked with more extensive profiling of transcriptional changes. This will be most practical using genome-wide measurements of pre-mRNA levels that may be possible from conventional mRNA sequencing at greater sequence depth (Gray et al. 2014), since the short timescales and stress treatments used here make protocols such as base analog labelling, RNA polymerase II ChIP sequencing, and global run-on sequencing impractical. Notably, however, pre-mRNA levels began decreasing during the stress period for all three genes assayed, regardless of changes in mRNA. This suggests an initial transcriptional burst, mediated by light-activated transcription factors, which lasts for approximately 30 minutes as observed in mammals and fungi in response to a stimulus (Molina et al. 2013; Li et al. 2018; Cesbron et al. 2015).

Transcriptome resetting during recovery appears to be determined in advance, during light stress, by changes in mRNA stability and transcription. As these are influenced by the duration of stress, it stands to reason that the recovery response may be altered in the same way. Among studies investigating recovery, it is rare that differing lengths of stress are compared. As demonstrated here, the recovery response is influenced by the duration of stress. Indeed, plants entering recovery after only ten minutes of light stress displayed steady transcript abundance (Figure S3). Plants required at least 30 minutes of light stress before observing the expected rapid decline, which coincides with the mRNA stability data showing transcripts were destabilised by this point. Given that transcription appears to be ongoing at 30 minutes, this suggests that transcript destabilisation is the primary response for regulation in recovery, with a secondary transcriptional shut-off occurring during recovery itself. This coordination of mRNA stability and transcription aligns with observations made in yeast responding to oxidative stress (Shalem et al. 2008; Molin et al. 2009), whereby early induced transcripts are destabilised while those repressed are stabilised. This appears to be a mechanism by which the organism ‘prepares’ for recovery; upon which the destabilised stress-induced transcripts are degraded while the stabilised stress-repressed transcripts accumulate, ultimately resetting the transcriptome to a pre-stress state.

While impairments in RNA decay enzymes, especially 5′ - 3′ pathways, are well documented in influencing plant stress responses by affecting steady-state mRNA stability (Xu and Chua 2012; Soma et al. 2017; Crisp et al. 2018; Merret et al. 2013; Jang et al. 2019; Yu et al. 2019; Wawer et al. 2018; Nguyen et al. 2015). The mechanism of transcript destabilisation, occurring during light stress, which facilitates RRGD remains unclear. Indeed, this has been challenging to identify since RNA decay pathways are complex and redundant, with mutant analyses complicated by both feedback, compensation and lethality of combinatorial mutations. Previous studies have profiled a series of combinatorial mutants during recovery,

however, down-regulation of stress-induced genes appeared unperturbed (Crisp et al. 2017; Armbruster et al. 2019). However, mRNA turnover is also regulated by numerous mRNA-binding proteins, interacting with translation and decay machinery, which require further exploration (Chantarachot and Bailey-Serres 2018).

Regulation of translation is evident during late light stress and at onset of recovery independent to changes in total mRNA

There is an increasing number of reports highlighting the regulation of translation in plants responding to stress, at both global and transcript-specific levels in conjunction with changes in mRNA turnover and stability (Chantarachot and Bailey-Serres 2018). Extending to this literature, we find that regulation of translation is dynamic during light stress and recovery. This was evident as transcript-specific changes in polysome-association (Figure S4 A-B), as opposed to wholesale reorganisation elicited by pattern-triggered immunity (bacterial translation elongation factor EF-Tu, elf18) (Xu et al. 2017), darkness (Juntawong and Bailey-Serres 2012), heat stress (Merret et al. 2017; Zhang et al. 2017), and hypoxia (Mustroph et al. 2009). The modesty in translational response observed here may reflect a stress of lesser intensity, in this case a 10-fold increase in light irradiance for 60 minutes. This posits greater complexity to the regulation of translation, at the global and transcript-specific levels, to be tuned based on environmental stimuli and requirements. This is likely determined through the action of intra-cellular signalling pathways and their interplay with RNA-binding proteins and translational machinery, which represents new avenues of investigation. Retrograde signalling has been linked to nuclear RNA processing (Zhao et al. 2020). However, the speed with which translational regulation occurs (e.g. within 7.5 minutes recovery, Figure S4 C) posits direct interaction between chloroplast-derived signals and cytosolic translation factors or interacting RNA-binding proteins, many of which are redox-sensitive (Huang et al. 2019; Moore et al. 2016).

Temporal differences in transcript-specific translation were clearly observable based on changes in RPL (Figure 4 B). During early stress, there was a slight bias toward decreased RPL, indicating translation repression of many genes. This aligns with observations that stress typically initially represses translation by perturbing translational machinery involved in initiation, scanning, and elongation (Bresson et al. 2020; Shalgi et al. 2013; Merret et al. 2015). On the other hand, we observed a striking increase in RPL during late stress that occurred independently of changes in total mRNA levels. This likely reflects the combination of two phenomena. In the first instance, this may reflect a transient pausing of elongation, without eliciting mRNA degradation, which resumes as cells begin to acclimate to the new conditions, as was observed in yeast (Shalgi et al. 2013). Simultaneously, preferential translation may be occurring for light stress-associated genes to facilitate an acclimatory response (Chen et al. 2021). The concordance between total and polysome-bound mRNA levels was also uncoupled rapidly upon transition to recovery, but is eventually re-established after 30 minutes (Figure S4 C). This reinforces the notion that this is an active period of regulation to establish post-stress homeostasis to favour growth, as opposed to a passive release of stress defence to return to a pre-stress condition. Indeed, although physiological and anatomical parameters return to pre-stressed levels after recovery from non-lethal stress, differential redox (Brossa et al. 2015), proteomic (Schneider et al. 2019; Tamburino et al. 2017; Lyon et al. 2016), and metabolomic (Wedeking et al. 2018; Lehmann et al. 2012) signatures represent a unique cellular environment especially during early recovery.

Translation and mRNA stability are coupled by a complex variety of interactions (Roy and Jacobson 2013). For instance, perturbations to translation, such as ribosome initiation, elongation, or unloading, can elicit changes to transcript stability in association with mRNA translation and degradation machinery. For instance, glucose withdrawal rapidly abolished 5’ RNA binding of translation initiation factors within 2 minutes, leading to translational shutdown without mRNA degradation (Bresson et al. 2020). Conversely, heat shock induced progressive loss of 5’ RNA binding of translation initiation factors paired with Xrn1-mediated mRNA degradation within 12 minutes (Bresson et al. 2020). Given the complexity of these interactions, it is unsurprising that we observed a negligible relationship between changes in RPL and stability (Figure 4 C). However, subsets of transcripts showed changes in polysome-association that were consistent with protection from degradation and co-translation decay. For example, many transcripts had altered RPL without significant changes in total mRNA abundance (e.g. 13.22% after 30 mins HL, Figure 4 B). At the same time, a smaller fraction (6.64% after 30 mins HL) of transcripts showed increased or unchanged RPL alongside decreased total mRNA abundance, possibly representing transcripts undergoing

co-translational decay. Contrary to expectations, we did not see evidence of elevated co-translation decay during recovery, with a similar proportion of transcripts having reduced mRNA abundance alongside unchanged, or increased, RPL (5.43%). Further, it was hypothesised that RRGD transcripts underwent co-translational decay during recovery, which we expected to observe as reduced RPL either during late stress or upon recovery. While declines in total mRNA of RRGD genes were generally concordant with declines in polysome-bound mRNA (Figure S5), RPL tended to increase during late stress in high light induced transcripts (Figure 5). Upon recovery, there was a notable decrease in RPL, especially for category 3 RRGD transcripts, suggesting that polysome-bound mRNAs were declining faster than free mRNAs, and therefore are likely undergoing co-translational decay. The incorporation of translational inhibitors with this experimental strategy, targeting initiation (Sekiyama et al. 2015) or elongation (Schneider-Poetsch et al. 2010), may help unpack the fate of light-induced transcripts when translation is perturbed.

Lastly, it was previously unclear the extent to which rapid changes in mRNA abundance would contribute to protein-level changes (Crisp et al. 2017). In general, we found that changes in polysome-bound mRNA levels correlated with those in the total mRNA pool. This was highlighted by temporal changes measured in previously defined RRGD loci (Figure 5, Figure S5). Therefore, transcript-level changes in total mRNA should translate to increased ribosome association, resulting in greater translation. Whether or not this would lead to gross changes in protein abundance is unclear, depending on the stability of the protein product (Li et al. 2017). Nonetheless, our observations suggest that the transcriptional compensation observed at genes encoding proteins degraded under high light, should result in elevated translation that contributes to maintaining proteostasis during stress (Li et al. 2022).

Tables

Table 1. Effect size parameters for differences in mRNA half-life between this study and other datasets

Comparison study	Mean difference (θ)	Median difference ($\mu_{1/2}$)	Cliff's delta (**δ**)
Narsai et al. 2007	180	131	0.946
Sorenson et al. 2018	94.8	52.4	0.808
Szabo et al. 2020	70.1	62.1	0.922
Chantarachot et al. 2020	352	94.8	0.858

Table 2. Effect sizes parameters for differences in mRNA half-life between conditions

Contrast	Mean difference (θ)	Median difference ($\mu_{1/2}$)	Cliff's delta (**δ**)
HL - US	-5.69	-4.21	-0.268
REC - US	-0.668	-0.509	-0.0326

Funding

This work was supported by the Australian Research Council (ARC) Laureate Fellowship (FL190100056) to BJP. ABS was supported by a PhD scholarship from the Grains Research and Development Council (GRS11010), and an Australian Research Training Program scholarship from the Australian Government. DRG was supported by funding from the CSIRO Synthetic Biology Future Science Platform. PAC was supported by an ARC Discovery Early Career Researcher Award (DE200101748).

Acknowledgements

We acknowledge the ACRF Biomolecular Resource Facility, a service node of Bioplatforms Australia, and the Centre for Biodiversity Analysis Ecogenomics and Bioinformatics Lab, both hosted at The Australian National University, for provision of resources and expertise to perform Illumina sequencing. This project was supported with the provision of plant growth facilities by the Australian Plant Phenomics Facility and computational infrastructure by the National Computational Infrastructure, both supported under the National Collaborative Research Infrastructure Strategy of the Australian Government.

References

Anderson SJ, Kramer MC, Gosai SJ, Yu X, Vandivier LE, Nelson ADL, Anderson ZD, Beilstein MA, Fray RG, Lyons E, et al. 2018. N6-Methyladenosine Inhibits Local Ribonucleolytic Cleavage to Stabilize mRNAs in Arabidopsis. *Cell Reports* **25**: 1146–1157.e3. http://dx.doi.org/10.1016/j.celrep.2018.10.020.

Arae T, Isai S, Sakai A, Mineta K, Yokota Hirai M, Suzuki Y, Kanaya S, Yamaguchi J, Naito S, Chiba Y. 2017. Co-ordinated Regulations of mRNA Synthesis and Decay during Cold Acclimation in Arabidopsis Cells. *Plant Cell Physiol* **58**: 1090–1102.

Armbruster L, Uslu VV, Wirtz M, Hell R. 2019. The Recovery from Sulfur Starvation Is Independent from the mRNA Degradation Initiation Enzyme PARN in Arabidopsis. *Plants* **8**. http://dx.doi.org/10.3390/plants8100380.

Armbruster U, Carrillo LR, Venema K, Pavlovic L, Schmidtmann E, Kornfeld A, Jahns P, Berry JA, Kramer DM, Jonikas MC. 2014. Ion antiport accelerates photosynthetic acclimation in fluctuating light environments. *Nat Commun* **5**: 5439.

Armbruster U, Leonelli L, Correa Galvis V, Strand D, Quinn EH, Jonikas MC, Niyogi KK. 2016. Regulation and Levels of the Thylakoid K+/H+ Antiporter KEA3 Shape the Dynamic Response of Photosynthesis in Fluctuating Light. *Plant Cell Physiol* **57**: 1557–1567.

Bates D, Mächler M, Bolker B, Walker S. 2015. Fitting Linear Mixed-Effects Models Usinglme4. *Journal of Statistical Software* **67**. http://dx.doi.org/10.18637/jss.v067.i01.

Bäurle I, Trindade I. 2020. Chromatin regulation of somatic abiotic stress memory. *J Exp Bot* **71**: 5269–5279.

Bielecka M, Watanabe M, Morcuende R, Scheible W-R, Hawkesford MJ, Hesse H, Hoefgen R. 2014. Transcriptome and metabolome analysis of plant sulfate starvation and resupply provides novel information on transcriptional regulation of metabolism associated with sulfur, nitrogen and phosphorus nutritional responses in Arabidopsis. *Front Plant Sci* **5**: 805.

Borsani O, Zhu J, Verslues PE, Sunkar R, Zhu J-K. 2005. Endogenous siRNAs derived from a pair of natural cis-antisense transcripts regulate salt tolerance in Arabidopsis. *Cell* **123**: 1279–1291.

Bray NL, Pimentel H, Melsted P, Pachter L. 2016. Near-optimal probabilistic RNA-seq quantification. *Nat Biotechnol* **34**: 525–527.

Bresson S, Shchepachev V, Spanos C, Turowski TW, Rappsilber J, Tollervey D. 2020. Stress-Induced Translation Inhibition through Rapid Displacement of Scanning Initiation Factors. *Mol Cell* **80**: 470–484.e8.

Brossa R, Pintó-Marijuan M, Francisco R, López-Carbonell M, Chaves MM, Alegre L. 2015. Redox proteomics and physiological responses in Cistus albidus shrubs subjected to long-term summer drought followed by recovery. *Planta* **241**: 803–822.

Cesbron F, Oehler M, Ha N, Sancar G, Brunner M. 2015. Transcriptional refractoriness is dependent on core promoter architecture. *Nat Commun* **6**: 6753.

Chan LY, Mugler CF, Heinrich S, Vallotton P, Weis K. 2018. Non-invasive measurement of mRNA decay

reveals translation initiation as the major determinant of mRNA stability. *Elife* **7**. http://dx.doi.org/10.7554/eLife.32536.

Chantarachot T, Bailey-Serres J. 2018. Polysomes, Stress Granules, and Processing Bodies: A Dynamic Triumvirate Controlling Cytoplasmic mRNA Fate and Function. *Plant Physiol* **176**: 254–269.

Chantarachot T, Sorenson RS, Hummel M, Ke H, Kettenburg AT, Chen D, Aiyetiwa K, Dehesh K, Eulgem T, Sieburth LE, et al. 2020. DHH1/DDX6-like RNA helicases maintain ephemeral half-lives of stress-response mRNAs. *Nat Plants* **6**: 675–685.

Chen Y, Liu M, Dong Z. 2021. Preferential Ribosome Loading on the Stress-Upregulated mRNA Pool Shapes the Selective Translation under Stress Conditions. *Plants* **10**. http://dx.doi.org/10.3390/plants10020304.

Chen Y, Lun ATL, Smyth GK. 2016. From reads to genes to pathways: differential expression analysis of RNA-Seq experiments using Rsubread and the edgeR quasi-likelihood pipeline. *F1000Res* **5**: 1438.

Chiba Y, Mineta K, Hirai MY, Suzuki Y, Kanaya S, Takahashi H, Onouchi H, Yamaguchi J, Naito S. 2013. Changes in mRNA stability associated with cold stress in Arabidopsis cells. *Plant Cell Physiol* **54**: 180–194.

Crisp PA, Ganguly D, Eichten SR, Borevitz JO, Pogson BJ. 2016. Reconsidering plant memory: Intersections between stress recovery, RNA turnover, and epigenetics. *Sci Adv* **2**: e1501340.

Crisp PA, Ganguly DR, Smith AB, Murray KD, Estavillo GM, Searle I, Ford E, Bogdanović O, Lister R, Borevitz JO, et al. 2017. Rapid Recovery Gene Downregulation during Excess-Light Stress and Recovery in Arabidopsis. *Plant Cell* **29**: 1836–1863.

Crisp PA, Smith AB, Ganguly DR, Murray KD, Eichten SR, Millar AA, Pogson BJ. 2018. RNA Polymerase II Read-Through Promotes Expression of Neighboring Genes in SAL1-PAP-XRN Retrograde Signaling. *Plant Physiol* **178**: 1614–1630.

Dean C, Leech RM. 1982. Genome Expression during Normal Leaf Development. *Plant Physiology* **69**: 904–910. http://dx.doi.org/10.1104/pp.69.4.904.

Desvoyes B, Ramirez-Parra E, Xie Q, Chua N-H, Gutierrez C. 2006. Cell type-specific role of the retinoblastoma/E2F pathway during Arabidopsis leaf development. *Plant Physiol* **140**: 67–80.

Donnelly PM, Bonetta D, Tsukaya H, Dengler RE, Dengler NG. 1999. Cell cycling and cell enlargement in developing leaves of Arabidopsis. *Dev Biol* **215**: 407–419.

Edgar R, Domrachev M, Lash AE. 2002. Gene Expression Omnibus: NCBI gene expression and hybridization array data repository. *Nucleic Acids Res* **30**: 207–210.

Elkon R, Zlotorynski E, Zeller KI, Agami R. 2010. Major role for mRNA stability in shaping the kinetics of gene induction. *BMC Genomics* **11**: 259.

Estavillo GM, Crisp PA, Pornsiriwong W, Wirtz M, Collinge D, Carrie C, Giraud E, Whelan J, David P, Javot H, et al. 2011. Evidence for a SAL1-PAP chloroplast retrograde pathway that functions in drought and high light signaling in Arabidopsis. *Plant Cell* **23**: 3992–4012.

Ge SX, Jung D, Yao R. 2020. ShinyGO: a graphical gene-set enrichment tool for animals and plants. *Bioinformatics* **36**: 2628–2629.

Gray JM, Harmin DA, Boswell SA, Cloonan N, Mullen TE, Ling JJ, Miller N, Kuersten S, Ma Y-C, McCarroll SA, et al. 2014. SnapShot-Seq: a method for extracting genome-wide, in vivo mRNA dynamics from a single total RNA sample. *PLoS One* **9**: e89673.

Hanson G, Alhusaini N, Morris N, Sweet T, Coller J. 2018. Translation elongation and mRNA stability are coupled through the ribosomal A-site. *RNA* **24**: 1377–1389.

Huang J, Willems P, Wei B, Tian C, Ferreira RB, Bodra N, Martínez Gache SA, Wahni K, Liu K, Vertommen D, et al. 2019. Mining for protein S-sulfenylation in uncovers redox-sensitive sites. *Proc Natl Acad Sci*

U S A **116**: 21256–21261.

Ishihara H, Obata T, Sulpice R, Fernie AR, Stitt M. 2015. Quantifying protein synthesis and degradation in Arabidopsis by dynamic 13CO2 labeling and analysis of enrichment in individual amino acids in their free pools and in protein. *Plant Physiol* **168**: 74–93.

Jang G-J, Yang J-Y, Hsieh H-L, Wu S-H. 2019. Processing bodies control the selective translation for optimal development of Arabidopsis young seedlings. *Proc Natl Acad Sci U S A* **116**: 6451–6456.

Jung H-S, Crisp PA, Estavillo GM, Cole B, Hong F, Mockler TC, Pogson BJ, Chory J. 2013. Subset of heat-shock transcription factors required for the early response of Arabidopsis to excess light. *Proc Natl Acad Sci U S A* **110**: 14474–14479.

Juntawong P, Bailey-Serres J. 2012. Dynamic Light Regulation of Translation Status in Arabidopsis thaliana. *Front Plant Sci* **3**: 66.

Juntawong P, Girke T, Bazin J, Bailey-Serres J. 2014. Translational dynamics revealed by genome-wide profiling of ribosome footprints in *Arabidopsis*. *Proceedings of the National Academy of Sciences* **111**. http://dx.doi.org/10.1073/pnas.1317811111.

Kersey PJ, Allen JE, Armean I, Boddu S, Bolt BJ, Carvalho-Silva D, Christensen M, Davis P, Falin LJ, Grabmueller C, et al. 2016. Ensembl Genomes 2016: more genomes, more complexity. *Nucleic Acids Res* **44**: D574–80.

Kramer MC, Janssen KA, Palos K, Nelson ADL, Vandivier LE, Garcia BA, Lyons E, Beilstein MA, Gregory BD. 2020. N ^{6} - methyladenosine and RNA secondary structure affect transcript stability and protein abundance during systemic salt stress in Arabidopsis. *Plant Direct* **4**. http://dx.doi.org/10.1002/pld3.239.

Kuznetsova A, Brockhoff PB, Christensen RHB. 2017. LmerTest package: Tests in linear mixed effects models. *J Stat Softw* **82**. http://www.jstatsoft.org/v82/i13/.

Lecampion C, Floris M, Fantino JR, Robaglia C, Laloi C. 2016. An Easy Method for Plant Polysome Profiling. *Journal of Visualized Experiments*. http://dx.doi.org/10.3791/54231.

Lefcheck JS. 2016. piecewiseSEM : Piecewise structural equation modelling in r for ecology, evolution, and systematics. *Methods in Ecology and Evolution* **7**: 573–579. http://dx.doi.org/10.1111/2041-210x.12512.

Lehmann M, Laxa M, Sweetlove LJ, Fernie AR, Obata T. 2012. Metabolic recovery of Arabidopsis thaliana roots following cessation of oxidative stress. *Metabolomics* **8**: 143–153.

Liao Y, Smyth GK, Shi W. 2014. featureCounts: an efficient general purpose program for assigning sequence reads to genomic features. *Bioinformatics* **30**: 923–930. http://dx.doi.org/10.1093/bioinformatics/btt656.

Liao Y, Smyth GK, Shi W. 2013. The Subread aligner: fast, accurate and scalable read mapping by seed-and-vote. *Nucleic Acids Res* **41**: e108.

Li C, Cesbron F, Oehler M, Brunner M, Höfer T. 2018. Frequency Modulation of Transcriptional Bursting Enables Sensitive and Rapid Gene Regulation. *Cell Syst* **6**: 409–423.e11.

Li H, Handsaker B, Wysoker A, Fennell T, Ruan J, Homer N, Marth G, Abecasis G, Durbin R, 1000 Genome Project Data Processing Subgroup. 2009. The Sequence Alignment/Map format and SAMtools. *Bioinformatics* **25**: 2078–2079.

Li L, Duncan O, Ganguly DR, Lee CP, Crisp PA, Wijerathna-Yapa A, Salih K, Trösch J, Pogson BJ, Millar AH. 2022. Enzymes degraded under high light maintain proteostasis by transcriptional regulation in. *Proc Natl Acad Sci U S A* **119**: e2121362119.

Li L, Nelson CJ, Trösch J, Castleden I, Huang S, Millar AH. 2017. Protein Degradation Rate in Leaf Growth and Development. *Plant Cell* **29**: 207–228.

Liu B, Qian S-B. 2014. Translational reprogramming in cellular stress response. *Wiley Interdiscip Rev RNA* **5**: 301–315.

Locke AM, Barding GA Jr, Sathnur S, Larive CK, Bailey-Serres J. 2018. Rice SUB1A constrains remodelling of the transcriptome and metabolome during submergence to facilitate post-submergence recovery. *Plant Cell Environ* **41**: 721–736.

Lyon D, Castillejo MA, Mehmeti-Tershani V, Staudinger C, Kleemaier C, Wienkoop S. 2016. Drought and Recovery: Independently Regulated Processes Highlighting the Importance of Protein Turnover Dynamics and Translational Regulation in Medicago truncatula. *Mol Cell Proteomics* **15**: 1921–1937.

Merret R, Carpentier M-C, Favory J-J, Picart C, Descombin J, Bousquet-Antonelli C, Tillard P, Lejay L, Deragon J-M, Charng Y-Y. 2017. Heat Shock Protein HSP101 Affects the Release of Ribosomal Protein mRNAs for Recovery after Heat Shock. *Plant Physiol* **174**: 1216–1225.

Merret R, Descombin J, Juan Y-T, Favory J-J, Carpentier M-C, Chaparro C, Charng Y-Y, Deragon J-M, Bousquet-Antonelli C. 2013. XRN4 and LARP1 are required for a heat-triggered mRNA decay pathway involved in plant acclimation and survival during thermal stress. *Cell Rep* **5**: 1279–1293.

Merret R, Nagarajan VK, Carpentier M-C, Park S, Favory J-J, Descombin J, Picart C, Charng Y-Y, Green PJ, Deragon J-M, et al. 2015. Heat-induced ribosome pausing triggers mRNA co-translational decay in Arabidopsis thaliana. *Nucleic Acids Res* **43**: 4121–4132.

Mickelbart MV, Hasegawa PM, Bailey-Serres J. 2015. Genetic mechanisms of abiotic stress tolerance that translate to crop yield stability. *Nat Rev Genet* **16**: 237–251.

Molina-Navarro MM, Castells-Roca L, Bellí G, García-Martínez J, Marín-Navarro J, Moreno J, Pérez-Ortín JE, Herrero E. 2008. Comprehensive transcriptional analysis of the oxidative response in yeast. *J Biol Chem* **283**: 17908–17918.

Molina N, Suter DM, Cannavo R, Zoller B, Gotic I, Naef F. 2013. Stimulus-induced modulation of transcriptional bursting in a single mammalian gene. *Proceedings of the National Academy of Sciences* **110**: 20563–20568. http://dx.doi.org/10.1073/pnas.1312310110.

Molin C, Jauhiainen A, Warringer J, Nerman O, Sunnerhagen P. 2009. mRNA stability changes precede changes in steady-state mRNA amounts during hyperosmotic stress. *RNA* **15**: 600–614.

Moore M, Gossmann N, Dietz K-J. 2016. Redox Regulation of Cytosolic Translation in Plants. *Trends Plant Sci* **21**: 388–397.

Munchel SE, Shultzaberger RK, Takizawa N, Weis K. 2011. Dynamic profiling of mRNA turnover reveals gene-specific and system-wide regulation of mRNA decay. *Mol Biol Cell* **22**: 2787–2795.

Muñoz A, Castellano MM. 2012. Regulation of Translation Initiation under Abiotic Stress Conditions in Plants: Is It a Conserved or Not so Conserved Process among Eukaryotes? *Comp Funct Genomics* **2012**: 406357.

Mustroph A, Zanetti ME, Jang CJH, Holtan HE, Repetti PP, Galbraith DW, Girke T, Bailey-Serres J. 2009. Profiling translatomes of discrete cell populations resolves altered cellular priorities during hypoxia in Arabidopsis. *Proc Natl Acad Sci U S A* **106**: 18843–18848.

Narsai R, Howell KA, Millar AH, O'Toole N, Small I, Whelan J. 2007. Genome-wide analysis of mRNA decay rates and their determinants in Arabidopsis thaliana. *Plant Cell* **19**: 3418–3436.

Nguyen AH, Matsui A, Tanaka M, Mizunashi K, Nakaminami K, Hayashi M, Iida K, Toyoda T, Van Nguyen D, Seki M. 2015. Loss of Arabidopsis 5′–3′ Exoribonuclease AtXRN4 Function Enhances Heat Stress Tolerance of Plants Subjected to Severe Heat Stress. *Plant and Cell Physiology* **56**: 1762–1772. http://dx.doi.org/10.1093/pcp/pcv096.

Pelechano V, Wei W, Steinmetz LM. 2015. Widespread Co-translational RNA Decay Reveals Ribosome Dynamics. *Cell* **161**: 1400–1412.

Pérez-Ortín JE, Alepuz PM, Moreno J. 2007. Genomics and gene transcription kinetics in yeast. *Trends*

Genet **23**: 250–257.

Pogson BJ, Ganguly D, Albrecht-Borth V. 2015. Insights into chloroplast biogenesis and development. *Biochimica et Biophysica Acta (BBA) - Bioenergetics* **1847**: 1017–1024. http://dx.doi.org/10.1016/j.bbabio.2015.02.003.

Ramakers C, Ruijter JM, Deprez RHL, Moorman AFM. 2003. Assumption-free analysis of quantitative real-time polymerase chain reaction (PCR) data. *Neurosci Lett* **339**: 62–66.

Risso D, Ngai J, Speed TP, Dudoit S. 2014. Normalization of RNA-seq data using factor analysis of control genes or samples. *Nature Biotechnology* **32**: 896–902. http://dx.doi.org/10.1038/nbt.2931.

Robinson MD, McCarthy DJ, Smyth GK. 2010. edgeR: a Bioconductor package for differential expression analysis of digital gene expression data. *Bioinformatics* **26**: 139–140. http://dx.doi.org/10.1093/bioinformatics/btp616.

Romero-Santacreu L, Moreno J, Pérez-Ortín JE, Alepuz P. 2009. Specific and global regulation of mRNA stability during osmotic stress in Saccharomyces cerevisiae. *RNA* **15**: 1110–1120.

Ross J. 1995. mRNA stability in mammalian cells. *Microbiol Rev* **59**: 423–450.

Roy B, Jacobson A. 2013. The intimate relationships of mRNA decay and translation. *Trends Genet* **29**: 691–699.

Ruijter JM, Ramakers C, Hoogaars WMH, Karlen Y, Bakker O, van den Hoff MJB, Moorman AFM. 2009. Amplification efficiency: linking baseline and bias in the analysis of quantitative PCR data. *Nucleic Acids Res* **37**: e45.

Schneider-Poetsch T, Ju J, Eyler DE, Dang Y, Bhat S, Merrick WC, Green R, Shen B, Liu JO. 2010. Inhibition of eukaryotic translation elongation by cycloheximide and lactimidomycin. *Nat Chem Biol* **6**: 209–217.

Schneider S, Turetschek R, Wedeking R, Wimmer MA, Wienkoop S. 2019. A Protein-Linger Strategy Keeps the Plant On-Hold After Rehydration of Drought-Stressed Beta vulgaris. *Frontiers in Plant Science* **10**. http://dx.doi.org/10.3389/fpls.2019.00381.

Schwartz DC, Parker R. 2000. mRNA decapping in yeast requires dissociation of the cap binding protein, eukaryotic translation initiation factor 4E. *Mol Cell Biol* **20**: 7933–7942.

Secco D, Wang C, Shou H, Schultz MD, Chiarenza S, Nussaume L, Ecker JR, Whelan J, Lister R. 2015. Stress induced gene expression drives transient DNA methylation changes at adjacent repetitive elements. *Elife* **4**. http://dx.doi.org/10.7554/eLife.09343.

Seeley KA, Byrne DH, Colbert JT. 1992. Red Light-Independent Instability of Oat Phytochrome mRNA in Vivo. *Plant Cell* **4**. https://pubmed.ncbi.nlm.nih.gov/12297628/ (Accessed August 30, 2021).

Sekiyama N, Arthanari H, Papadopoulos E, Rodriguez-Mias RA, Wagner G, Léger-Abraham M. 2015. Molecular mechanism of the dual activity of 4EGI-1: Dissociating eIF4G from eIF4E but stabilizing the binding of unphosphorylated 4E-BP1. *Proc Natl Acad Sci U S A* **112**: E4036–45.

Shalem O, Dahan O, Levo M, Martinez MR, Furman I, Segal E, Pilpel Y. 2008. Transient transcriptional responses to stress are generated by opposing effects of mRNA production and degradation. *Molecular Systems Biology* **4**: 4. http://dx.doi.org/10.1038/msb.2008.59.

Shalgi R, Hurt JA, Krykbaeva I, Taipale M, Lindquist S, Burge CB. 2013. Widespread regulation of translation by elongation pausing in heat shock. *Mol Cell* **49**: 439–452.

Sheikh MS, Saeed Sheikh M, Fornace AJ. 1999. Regulation of translation initiation following stress. *Oncogene* **18**: 6121–6128. http://dx.doi.org/10.1038/sj.onc.1203131.

Soma F, Mogami J, Yoshida T, Abekura M, Takahashi F, Kidokoro S, Mizoi J, Shinozaki K, Yamaguchi-Shinozaki K. 2017. ABA-unresponsive SnRK2 protein kinases regulate mRNA decay under osmotic stress in plants. *Nat Plants* **3**: 16204.

Soneson C, Love MI, Robinson MD. 2015. Differential analyses for RNA-seq: transcript-level estimates improve gene-level inferences. *F1000Res* **4**: 1521.

Sorenson RS, Deshotel MJ, Johnson K, Adler FR, Sieburth LE. 2018. mRNA decay landscape arises from specialized RNA decay substrates, decapping-mediated feedback, and redundancy. *Proc Natl Acad Sci U S A* **115**: E1485–E1494.

Steffens A, Bräutigam A, Jakoby M, Hülskamp M. 2015. The BEACH Domain Protein SPIRRIG Is Essential for Arabidopsis Salt Stress Tolerance and Functions as a Regulator of Transcript Stabilization and Localization. *PLoS Biol* **13**: e1002188.

Szabo EX, Reichert P, Lehniger M-K, Ohmer M, de Francisco Amorim M, Gowik U, Schmitz-Linneweber C, Laubinger S. 2020. Metabolic Labeling of RNAs Uncovers Hidden Features and Dynamics of the Arabidopsis Transcriptome. *Plant Cell* **32**: 871–887.

Tamburino R, Vitale M, Ruggiero A, Sassi M, Sannino L, Arena S, Costa A, Batelli G, Zambrano N, Scaloni A, et al. 2017. Chloroplast proteome response to drought stress and recovery in tomato (Solanum lycopersicum L.). *BMC Plant Biol* **17**: 40.

Wawer I, Golisz A, Sulkowska A, Kawa D, Kulik A, Kufel J. 2018. mRNA Decapping and 5’-3' Decay Contribute to the Regulation of ABA Signaling in. *Front Plant Sci* **9**: 312.

Wedeking R, Maucourt M, Deborde C, Moing A, Gibon Y, Goldbach HE, Wimmer MA. 2018. 1H-NMR metabolomic profiling reveals a distinct metabolic recovery response in shoots and roots of temporarily drought-stressed sugar beets. *PLoS One* **13**: e0196102.

Xu G, Greene GH, Yoo H, Liu L, Marqués J, Motley J, Dong X. 2017. Global translational reprogramming is a fundamental layer of immune regulation in plants. *Nature* **545**: 487–490.

Xu J, Chua N-H. 2012. Dehydration stress activates Arabidopsis MPK6 to signal DCP1 phosphorylation. *EMBO J* **31**: 1975–1984.

Yeung E, van Veen H, Vashisht D, Sobral Paiva AL, Hummel M, Rankenberg T, Steffens B, Steffen-Heins A, Sauter M, de Vries M, et al. 2018. A stress recovery signaling network for enhanced flooding tolerance in. *Proc Natl Acad Sci U S A* **115**: E6085–E6094.

Yu X, Li B, Jang G-J, Jiang S, Jiang D, Jang J-C, Wu S-H, Shan L, He P. 2019. Orchestration of Processing Body Dynamics and mRNA Decay in Arabidopsis Immunity. *Cell Rep* **28**: 2194–2205.e6.

Zeisel A, Köstler WJ, Molotski N, Tsai JM, Krauthgamer R, Jacob-Hirsch J, Rechavi G, Soen Y, Jung S, Yarden Y, et al. 2011. Coupled pre-mRNA and mRNA dynamics unveil operational strategies underlying transcriptional responses to stimuli. *Mol Syst Biol* **7**: 529.

Zhang L, Liu X, Gaikwad K, Kou X, Wang F, Tian X, Xin M, Ni Z, Sun Q, Peng H, et al. 2017. Mutations in eIF5B Confer Thermosensitive and Pleiotropic Phenotypes via Translation Defects in. *Plant Cell* **29**: 1952–1969.

Zhao X, Huang J, Chory J. 2020. Unraveling the Linkage between Retrograde Signaling and RNA Metabolism in Plants. *Trends Plant Sci* **25**: 141–147.

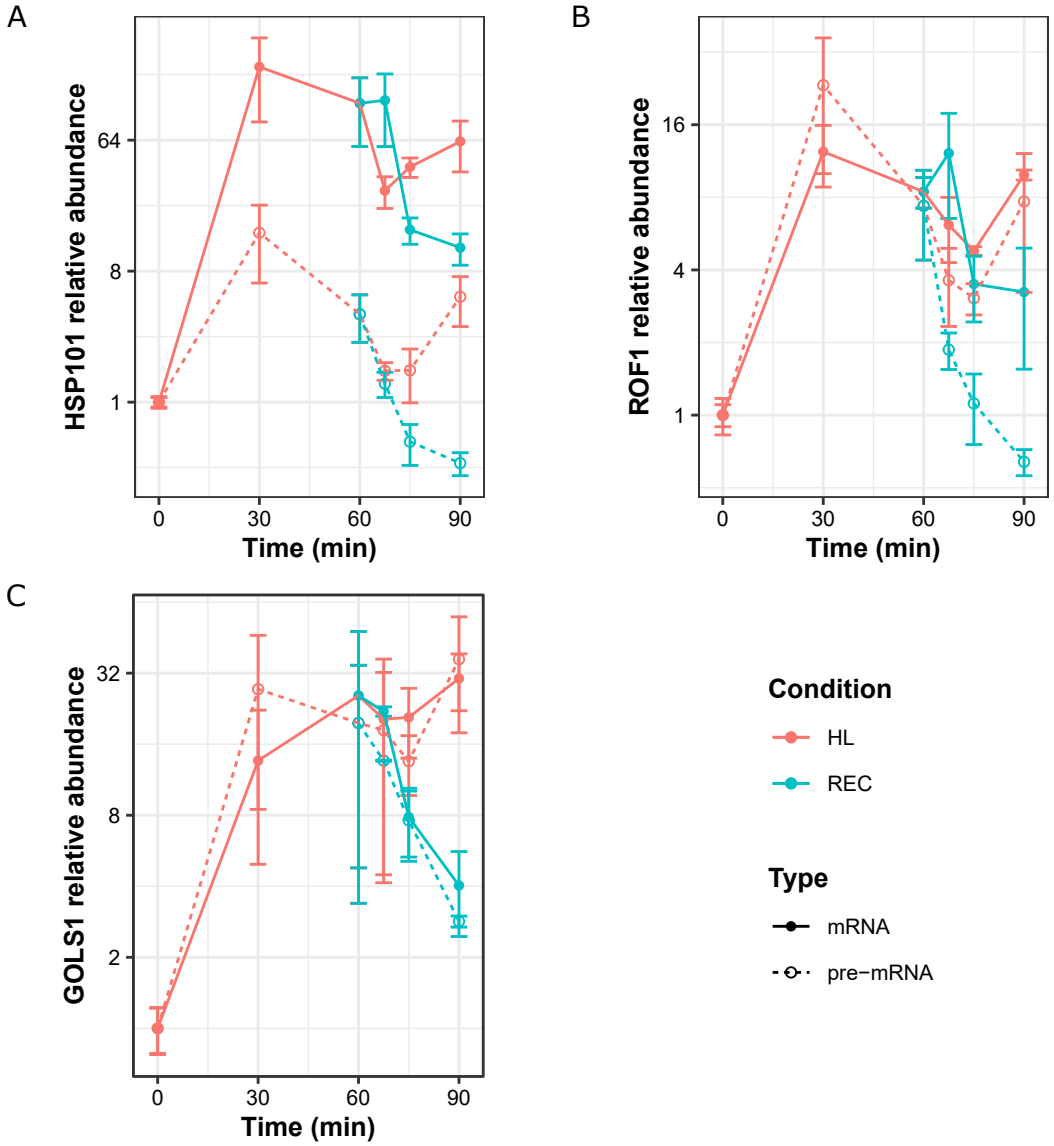

Figure S1 Pre-mRNA levels decrease more rapidly during recovery than mRNA (A-C) Profiles of pre-mRNA and mRNA for *HSP101*, *ROF1*, and *GOLS1* during HL and REC. Data is presented as relative abundance compared to time 0. Points denote means, error bars denote standard error of the mean (n=3).

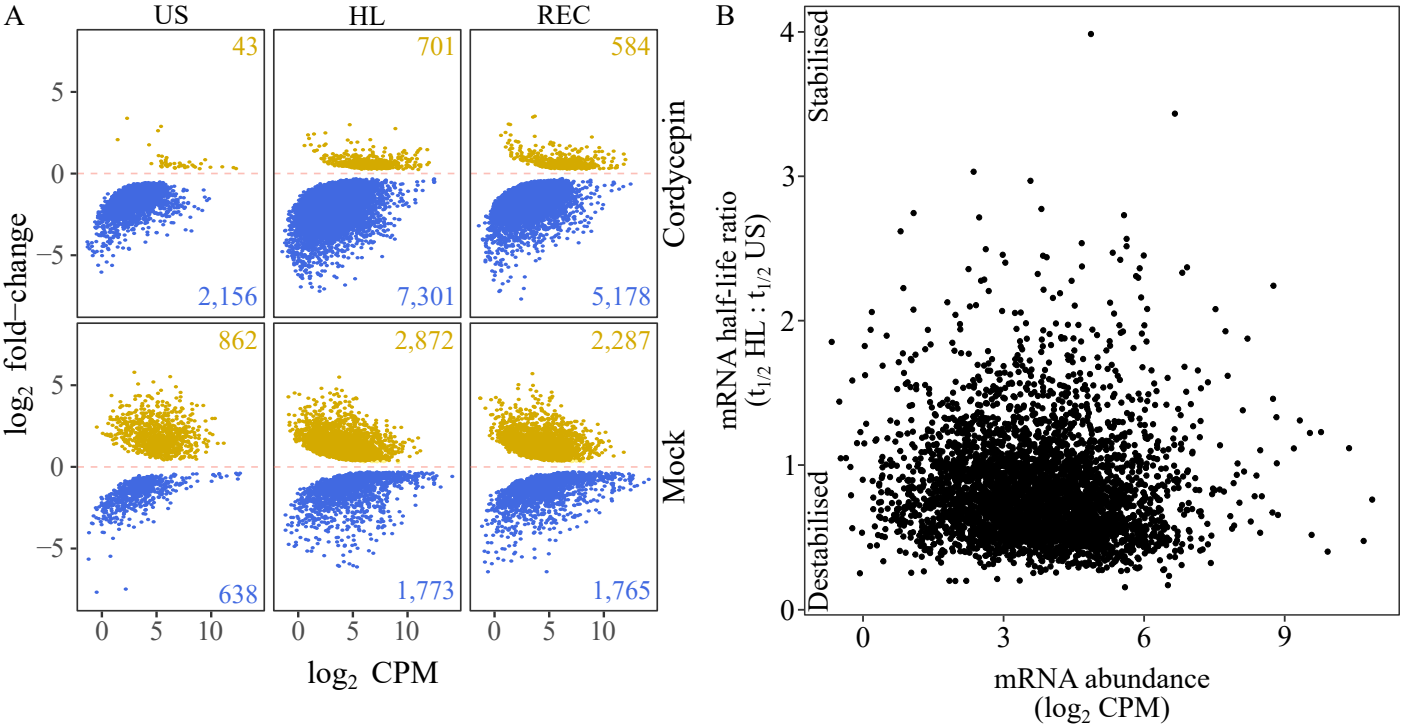

Figure S2 Syringe-infiltration of cordycepin facilitates modeling half-lives for transcripts of varying abundance

(A) Differential gene expression between 30 and 10 minutes post-infiltration with cordycepin or mock buffer in US, HL, or REC. Up- and down-regulated genes ($p < 0.05$) are denoted by yellow and blue points, respectively.

(B) Scatter plot relating the half-life ratio (HL/US) to mean mRNA abundance for 3,960 modelled transcripts. Points represent individual genes.

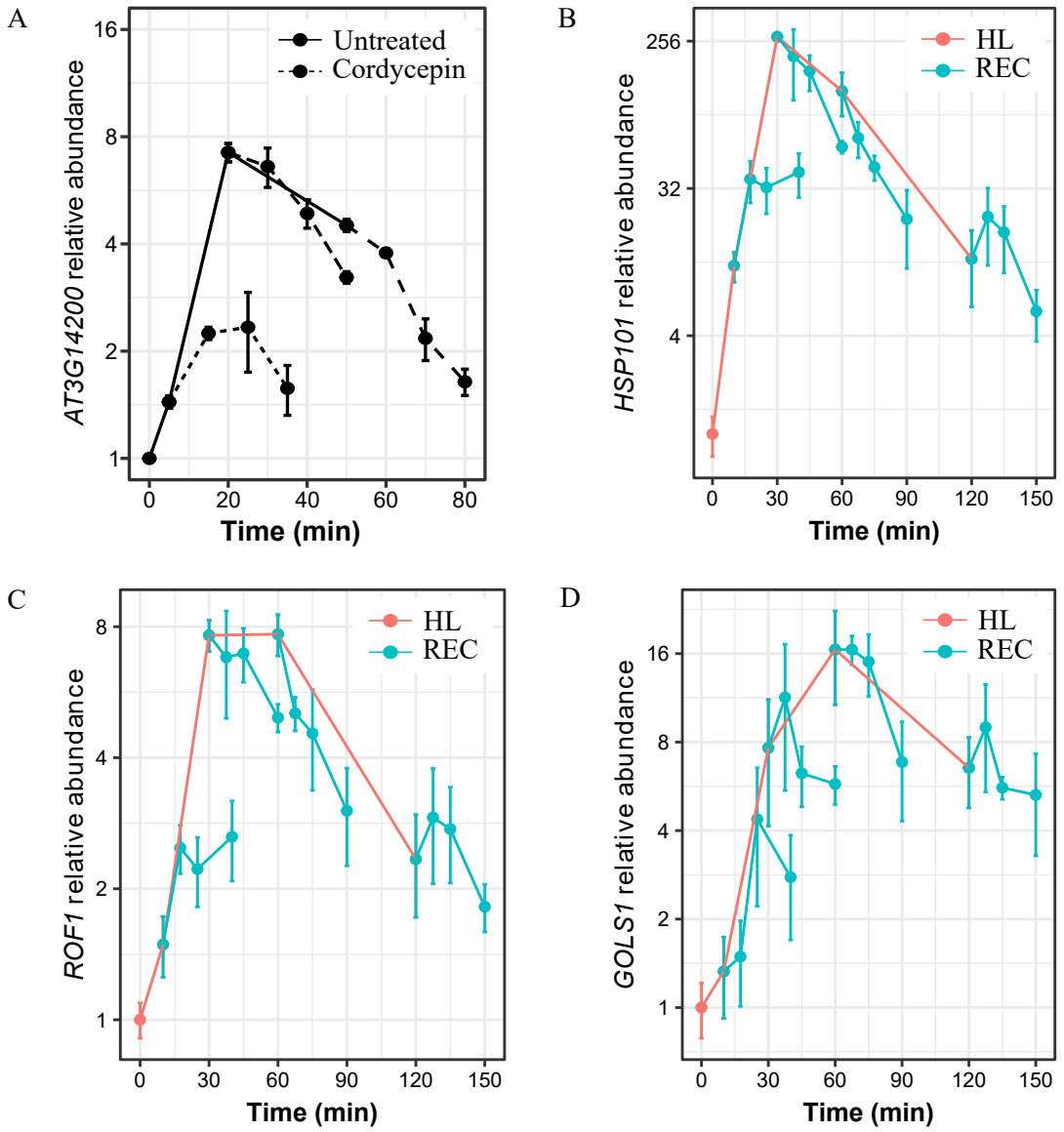

Figure S3 Rapid recovery gene down-regulation is dependent on length of HL
(A) Gene expression changes in AT3G14200 following cordycepin infiltration carried out at 5, 20, and 50 minutes HL. Solid line denotes untreated leaves, dashed line denotes cordycepin-infiltrated samples.
(B-D) Gene expression profiles of *HSP101*, *ROF1*, and *GOLS1* during REC after various lengths of HL. Red lines denote HL, blue lines denote REC (initiated at 10, 30, 60, and 120 minutes).
Points denote means, error bars denote standard error of the mean (n = 3).

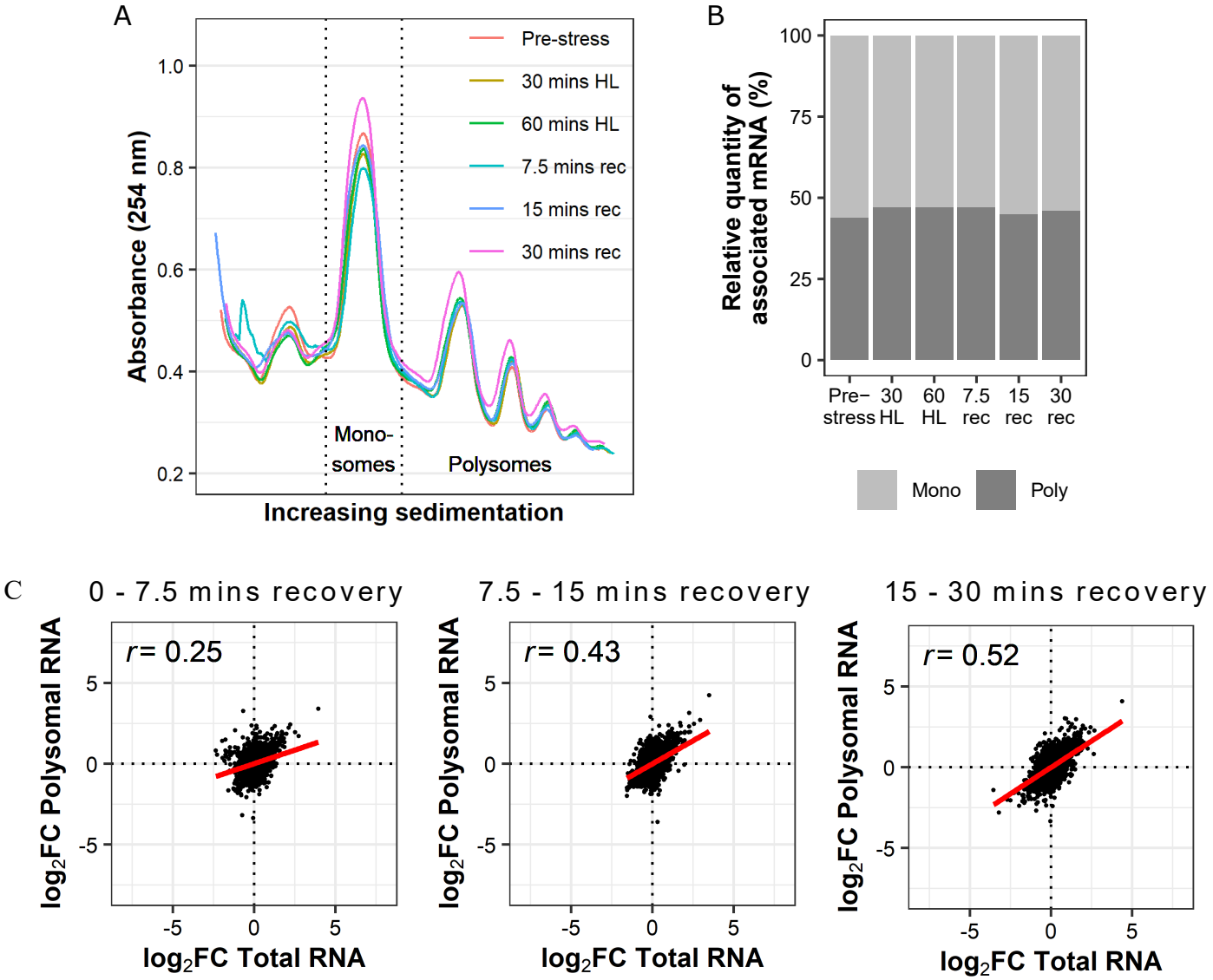

Figure S4 Uncoupling of total and polysome-bound RNA abundance during early recovery
(A) Monosomes and polysomes extracted from Arabidopsis seedlings were separated using gradient centrifugation and quantified by absorbance at 254 nm.
(B) Relative abundance of monosomes and polysomes was calculated by integration of the area under the absorbance profile.
(C) Correlation between changes in total and polysome-bound mRNA abundance between recovery time points. r denotes Pearson's correlation coefficient.

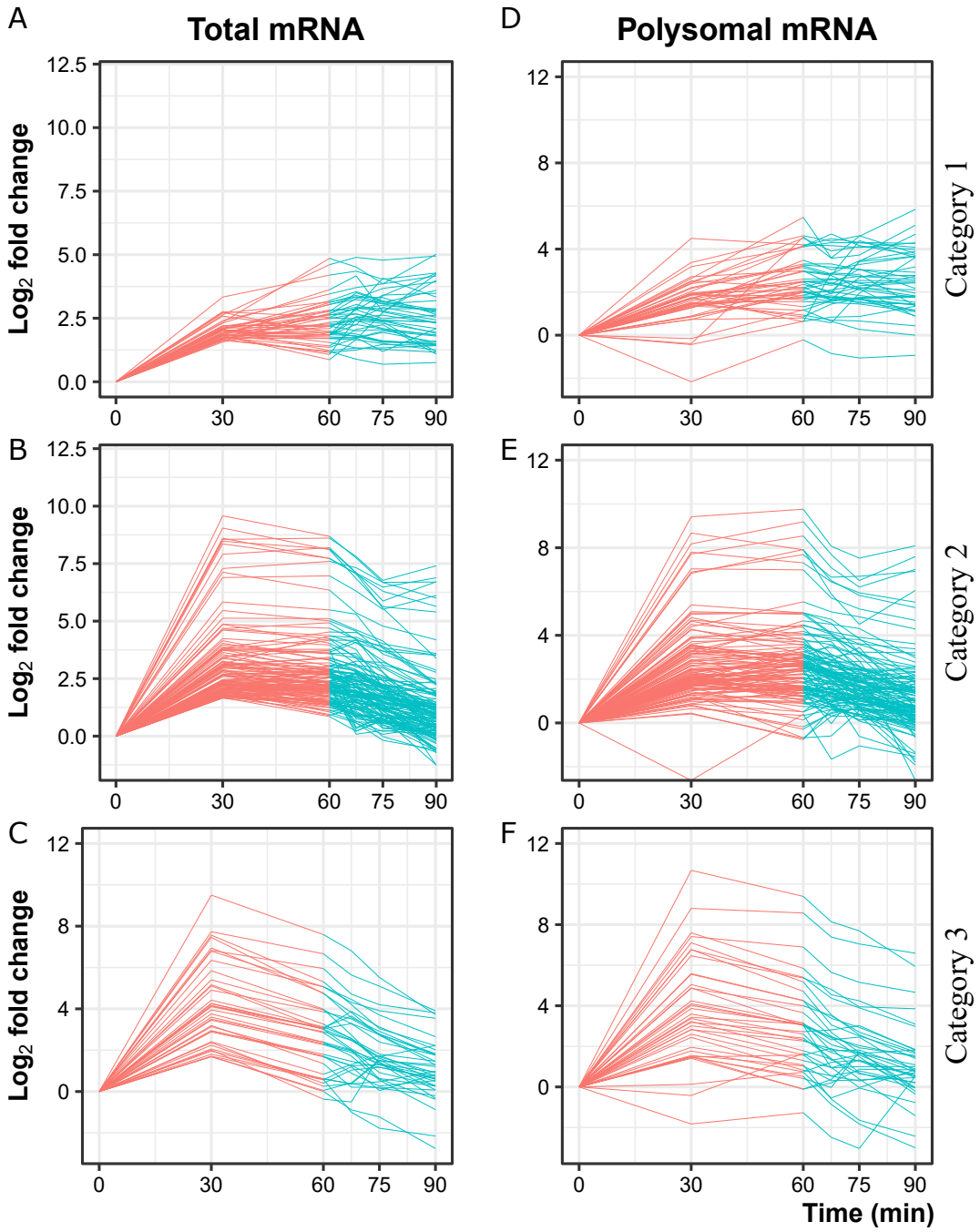

Figure S5 Expression profiles of light-induced total and polysome-associated mRNAs during light stress and recovery
(A-C) Genes induced by HL (FC > 3 after 30 mins) were categorised by their expression profiles in the total mRNA fraction. Category 1 genes remained elevated during REC. Category 2 genes were significantly down-regulated during REC. Category 3 genes were significantly down-regulated between 30 and 60 minutes HL.
(D-F) The corresponding changes in polysome-bound mRNA are displayed.
Lines represent mean relative abundance over time during HL (red) and REC (blue).